SYNTHESIS, CHARACTERIZATION OF CdS_xSe_{1-x} QUANTUM DOTS AND EVALUATION OF THEIR REAL-TIME MOTIONS IN LIVE CELLS

A Thesis Submitted to
the Graduate School of Engineering and Sciences of
İzmir Institute of Technology
in Partial Fulfillment of the Requirements for the Degree of

MASTER OF SCIENCE

in Chemistry

by
Gülçin ÜNAL

July 2011
İZMİR

We approve the thesis of **Gülçin ÜNAL**

Prof. Dr. Serdar ÖZÇELİK

Supervisor

Prof. Dr. Neşe ATABEY

Committee Member

Assoc. Prof. Dr. Bilge KARAÇALI

Committee Member

7 July 2011

Prof. Dr. Serdar ÖZÇELİK

Head of the Department of Chemistry

Prof. Dr. Durmuş Ali DEMİR

Dean of the Graduate School of Engineering and Sciences

ACKNOWLEDGEMENTS

First of all, I would like to express my gratitude to my supervisor Prof. Dr. Serdar ÖZÇELİK. He was a great person and scientist as well. After each discussion on this study, he made me more motivated and willing thanks to his knowledge and valuable comments.

I am thankful to Caner ÜNLÜ for his helps and guidance in my undergraduate and graduate studies. He always found solutions to my problems about thesis study. I thank to Leyla ERAL DOĞAN for her great comments and answers to all of my questions about chemistry, future plans, life… I also thank to Dr. Aslı TOYLU for sparing her time to train me for cell culture studies in a patient manner.

I would like to thank specially to my love Onur TOSUN for being such a great partner. His endless care and logical approaches were the best motivation for me. He was the biggest support to me in seven-year İYTE story.

Last, but not least, I appreciate my endless thanks to my great family. My father Cihat is very special person for me. He built his whole life around me and my brother. My mother Güler raised me for her lovely care. She always agreed with me in my wishes and decisions. It was great that she never gave up waking me up in the mornings for seven years also her prayers made me feel better. I thank to my brother Cihan who always shared his everything with me and also listening me about everyhing.

ABSTRACT

SYNTHESIS, CHARACTERIZATION OF CdS_xSe_{1-x} QUANTUM DOTS AND EVALUATION OF THEIR REAL-TIME MOTIONS IN LIVE CELLS

The use of quantum dots as fluorescent labels in bioimaging is the most intensively studied subject. The aim of this study is to elucidate locations of quantum dots and track their motions in real time through confocal microscopy and to evaluate influence of surface chemistry on diffusions of quantum dots in live cells. In this study, trioctylphosphine oxide (TOPO) capped CdS_xSe_{1-x} quantum dots were synthesized and then TOPO molecules were exchanged with 3-mercaptopropionic acid and N-acetyl-L-cysteine to make quantum dots water dispersible for cellular imaging. Human lung adenocarcinoma epithelial cells (A549) and human bronchial epithelial cells (BEAS-2B) were incubated 1 hour with CdS_xSe_{1-x} quantum dots with a concentration range of 1-10 μg/mL. Localizations and real time motions of quantum dots were tracked by a spinning disc confocal microscope. The center of fluorescent spots of quantum dots was determined by 2D Gaussian fitting with a sub-pixel resolution (<100nm/pixel). The mean square displacements, diffusion coefficients and trajectories in which quantum dots made motions were analyzed by the software ImageJ with a plug in Spot Tracker. Confocal images showed that both MPA and NAC cappped quantum dots were observed in the cytoplasm of cells. Trajectories of quantum dots in cellular environment demonstrated that the quantum dots performed various types of motions in live cells. Unimodal, trimodal and multimodal distribution histograms of the diffusion coefficeints were obtained for different capping agents (MPA and NAC) and cell types (A549 and BEAS-2B). We conclude that the surface chemistry regulates the motion of the quantum dots in the cellular environment.

ÖZET

CdS_xSe_{1-x} KUANTUM NOKTALARIN SENTEZİ, KARAKTERİZASYONU VE CANLI HÜCRELERDEKİ GERÇEK ZAMANLI HAREKETLERİNİN İNCELENMESİ

Bu çalışmada trioktilfosfin oksit (TOPO) kaplı CdS_xSe_{1-x} kuantum noktalar sentezlenmiş ve karakterize edilmiştir. Sentezlenen kuantum noktaların canlı hücreler içerisindeki gerçek zamanlı hareketleri izlenmiş ve yüzey kimyasının kuantum noktaların difüzyonları üzerindeki etkisi incelenmiştir. Kuantum noktaların hücre görüntüleme çalışmalarında kullanılabilmesi için suda çözünür hale getirilmesi gerekmektedir. Bu amaçla, yüzeydeki TOPO molekülleri 3-merkaptopropionik asit (MPA) ve N-asetil-L-sistein (NAC) ile değiştirilmiştir. Sağlıklı ve kanserli akciğer epitel hücre hatları sırasıyla (A549) ve (BEAS-2B), 1-10 μg/mL derişime sahip CdS_xSe_{1-x} kuantum noktalar ile 1-2 saat muamele edildikten sonra taramalı disk konfokal mikroskopta gözlem yapılmıştır. Parçacıkların gerçek zamanlı hareketleri ve konumları ImageJ programı içinde kullanılabilen Spot Tracker adlı eklenti ile yapılmıştır. MPA ve NAC kaplı CdS_xSe_{1-x} kuantum noktaların A549 ve BEAS-2B hücrelerinin sitoplazmasında bulunduğu konfokal mikroskop görüntüleri ile kanıtlanmıştır. Kuantum noktaların hücre ortamında izledikleri yollar, parçacıkların çeşitli difüzyon tiplerine sahip olduğunu göstermektedir. Kuantum noktaların yüzey kimyası ve muamele edilen hücre tipi değiştiğinde farklı türde hareketler gözlemlenmiştir. Ayrıca deney süresince kuantum noktaların hücre ortamındaki parlaklığında bir azalma olmadığı belirlenmiştir.

TABLE OF CONTENTS

LIST OF FIGURES

Figure **Page**

LIST OF TABLES

Table **Page**

CHAPTER 1

INTRODUCTION

1.1. Quantum Dots and Nanobiotechnology

Today's one of the most important fields of science is nanotechnology which is the study of manipulating matter at the nanoscale. It involves design, investigation, construction of systems at atomic and molecular scale. Another promising research field of current day is biotechnology, which is a part of applied biology that deals with using of living organisms in the areas requiring bioproducts. Nanobiotechnology combines these two areas in order to create nanobiosystems to meet a variety of challenges covering multiple applications. It is an interdisciplinary field combining biological, chemical and physical properties (Amin, Hwang, and Park 2011). Nanobiotechnology is advanced in recent years by incorporation of nanomaterials with biomaterials. Among various nanomaterials, quantum dots (QDs) attracted much attention in nanobiotechnology. Quantum dots are luminescent semiconductor nanocrystals and attracted much interest from various research communities due to their unique and tunable optical properties (Swafford et al. 2006). They exhibit quantum confinement effect which gives rise to unique optical properties in quantum dots, also giving them numerous advantages over current fluorophores, such as organic dyes and fluorescent proteins (Liang et al. 2010). Quantum dots possess narrow emission spectra tunable through visible and near-infrared wavelengths. They have large molar extinction coefficient, large Stoke's shift and narrow full width at half maximum. Beside these properties, quantum dots exhibit impressive photostability and high resistance against photobleaching which allows long term observations of biomolecules (Drbohlavova et al. 2009).

1.2. Confocal Microscopy

A microscope is an instrument which is used to see details that can not be detected by naked eye. A microscope must succeed in doing three functions: create a magnified image of the sample (magnification), separate the details in the image (resolution) and make the details visible to the naked eye or camera (contrast) (Abramowitz 2006).

The first invented microscope was the optical microscope, commonly referred as light microscope. It was invented in the 1600's by Anton Van Leeuwenhoek. It had one or more lenses in order to produce an amplified image of a specimen in the focal plane. Typical magnification of an optical microscope is up to 1500x with a theoretical resolution limit of around 200 nanometers. Although an optical microscope is the most widely used microscope, the most rapidly developing microscopy is fluorescence microscopy (Prasad, Semwogerere, and Weeks 2007).

The basic function of a fluorescence microscope is that the specimen is irradiated at a specific wavelength and then weaker emitted fluorescence from the excitation light is separated. In Figure 1.1, simple set up of fluorescence microscope is seen, excitation light is blue while emitted light is green. Dichroic mirror is used to reflect light shorter than a certain wavelength but transmit light of longer wavelength. Therefore, light from main source is reflected, passed through the objective to the sample. Light from specimen is passed through the objective and the dichroic mirror (Semwogerere and Weeks 2005).

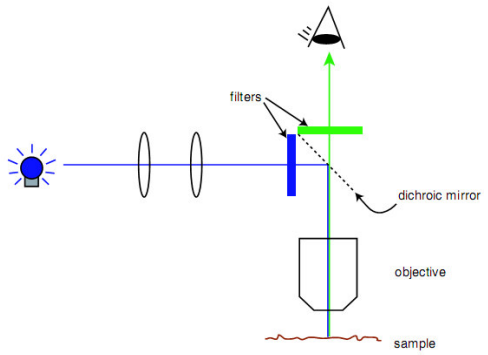

Figure 1.1. Simple set up of a fluorescence microscope.
(Source: Semwogerere et al. 2005*)*

Fluorescence microscopy has become a must in many research areas including biology, medicine, material science, etc. Its superiority is based on its unique properties which are not possible through other optical microscopes. It is possible to identify cells and submicroscopic cellular components by using fluorophores, component of a molecule which causes a molecule to be fluorescent, with a high specificity among nonfluorescing materials. The fluorescence microscope can show the presence of fluorescing materials with excellent sensitivity. Moreover, it can reveal the presence of single molecule by making multiple fluorescence staining (Lichtman and Conchello 2005). Fluorescence microscope has widely used however popularity of confocal microscopy increases day by day. Figure 1.2 shows the fluorescence microscope and confocal microscope relatively.

Confocal microscope was invented and also patended by Marvin Minsky in 1957 while he was a postdoctoral fellow at Harvard University (Minsky 1988). There has been a notable increase in the popularity of confocal microscopy in recent years because of its great applications in many research areas and many advantages over optical microscopy such as controllable depth of field, the elimination of image, degrading out-of-focus information and the ability to collect serial optical sections from thick specimen.

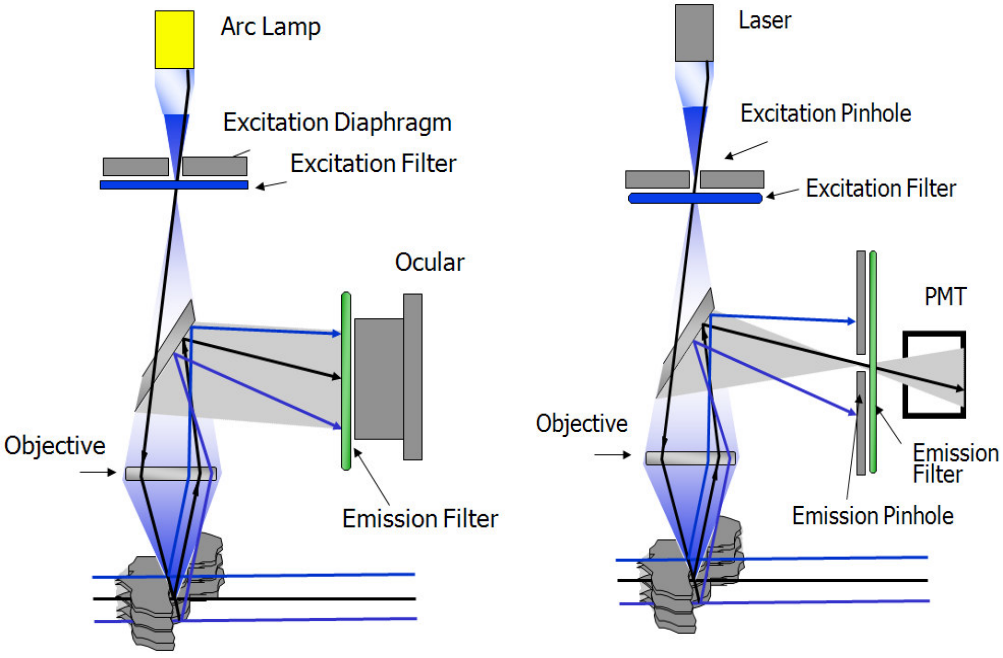

Figure 1.2. Simple set up of a fluorescence microscope and confocal microscope. (Source: Hubbard 2007)

The most important feature of a confocal microscope is its capability to isolate and collect a plane of focus from within a sample, eliminating the out of focus "haze" normally seen with a fluorescent sample. Fine detail is often obscured by the haze and can not be detected in a nonconfocal fluorescent microscope. Figure 1.3 will be descriptive to explain how confocal microscope operates.

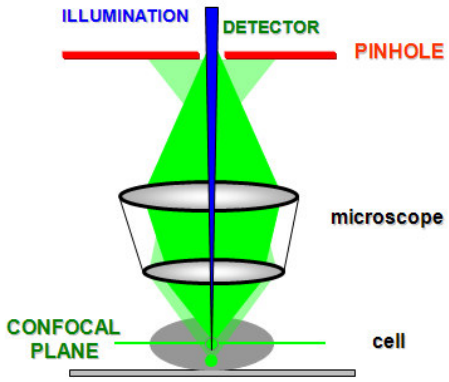

Figure 1.3. Schematic representation of illumination and detection through the pinhole. (Source: Hubbard 2007)

Basically illumination via a laser source is passed through a pinhole. The light from the pinhole is focussed to a particular point in the sample. Light passes deeper into the sample (pale green line) causing fluorescence emission from the sample below the confocal plane. The light from this point does not pass back through the pinhole and the detector ignores it. Emitted light from the focused point, at the confocal plane, passes in its entirety back through the pinhole and the detector uses it to form the image. Thus light from out of focus planes is discarded and does not form part of the image. However we need to scan that point of light. It can be done by keeping the point of light in a fixed place and moving the sample around it using a scanning stage. This is slow and not convenient for living biology as it shakes the sample around. A very popular method is to move the point of light using galvo driven mirrors. The point of light is rastered across and down the sample and an image is built up point by point. A third way is to move the pinhole or pinholes. By having a field of light and an array of pinholes in that field, the light is formed into a point or many points. By moving the

pinholes many points of light are scanned. This is the scanning disk principle and it produces the confocal image.

Spinning disk confocal microscope was developed by Eggar and Petran in late 1960s. In scanning disk microscope, the disk is located in a conjugate image plane and a partial rotation of the disk scans the specimen with thousands of beams of light that can cover all of the image plane. Multiple pinholes allow the specimen to be sampled in parallel. This produces a multiplicative gain in potential scan speed proportional to the number of pinholes present in the system. Another advantage of disk scanning is less photobleaching due to lower local excitation intensity. Moreover, there is no strict requirement for laser illumination, reducing cost and allowing more choices of excitation wavelengths.

However there exist some factors to be taken into consideration when using a disk scanning confocal microscope. Firstly, light fluoresced by structures away from the focus plane can reach to the detector through an adjacent pinhole, causing decrease in resolution of the microscope in z-direction. Secondly, low transmission of the light through the disk may hinder imaging of dim fluorescent samples. Thirdly, disc scanning confocal microscopes do not allow high power illumination of interested region for fluorescent recovery after photobleaching experiments (Chong et al. 2004).

Usage of confocal microscope in live cells is very important application of this system. In live cell imaging studies, experimenter must not harm the cells. The main difficulty in live cell microscopy is not to get an image but to do so without disturbing the cells. Moreover imaging should be carried out on a biological system that retains normal function. Usually, environmental variables like pH, CO_2 and temperature must be regulated. Collecting as much of the emitted fluorescence is very important since photodynamic damage and consequent change in cell behaviour is possible. Besides from these, it is important that all living processes have a characteristic time period, imaging system must create images at appropriate rate to be able to observe changes involved (Adams et al. 2003).

1.3. The Purpose of This Study

The purpose of the study is to synthesize and characterize water dispersible CdS_xSe_{1-x} quantum dots and to evaluate their real time motions in live cells through confocal microscopy. We will investigate the effect of surface chemistry of QDs on their motions.

1.4. Tracking Motions of Quantum Dots

The use of quantum dots as fluorescent labels in bioimaging is the most intensively studied subject and the first milestone application of quantum dots in bioimaging was reported by Alivisatos' group (Wang, Tang, and Kotov 2005). However it is crucial to determine the behaviour of quantum dots in cellular environment quantitatively by tracking their motions in real time. Intracellular diffusion pathways, localizations and diffusion types must be determined to ensure the use of quantum dots in biological applications. For this purpose, Image Processing and Analysis in JAVA (ImageJ) analysis program was used. ImageJ is a public domain, Java based image processing program, developed by National Institutes of Health (NIH). This program supports all common image manipulations including reading and writing of image files and operations on individual pixels, image regions and whole images. It can perform basic operations such as histogram and particle analysis and color manipulation. ImageJ can also calculate area and pixel value statistics of user defined selections. It is possible to measure distances and create density histograms and line profile plots using ImageJ. Functionality of ImageJ can be expanded through the use of plugins written in Java. Plugins are external programs that do not exist in core capabilities of ImageJ. In our analysis, spot tracker which is a plugin of ImageJ, was used to analyze motions of quantum dots in cells.

Confocal microscopy images of quantum dots in live cells appear as fluorescent spots. The center of fluorescent spots of nanoparticles was determined by 2D Gaussian fiiting by sub-pixel resolution using the Equation 1.1 (Bannai et al. 2006).

$$I(x,y) = A\exp\left\{\frac{[\ (x - x_0)^2 \quad (y - y_0)^2\ ]}{2\sigma^2}\right\} + B \tag{1.1}$$

The positions of fluorescent spots were determined in each image and the two-dimensional trajectories of quantum dots were calculated using position of spots in x and y directions. In Figure 1.4 an example of spot tracker result is seen.

Spot Tracker Results

File Edit Font

image	x spot [px]	y spot [px]	Conf. [%]	Pixel value	Velocity [pix/frame]	Mean intensity over 1x1 pixels window
1	2.79	7.59	93	225	0.00	225.0
2	2.82	7.61	94	214	0.04	213.5
3	2.96	7.64	92	218	0.15	217.7
4	3.43	7.61	92	230	0.47	230.0
5	3.36	7.58	79	206	0.08	206.2
6	3.60	7.19	79	237	0.46	237.3
7	3.74	7.22	78	242	0.15	242.3
8	5.35	6.70	90	240	1.69	239.7
9	4.79	7.53	95	228	1.00	228.2
10	4.52	7.48	96	244	0.28	244.2
11	4.50	6.50	91	252	0.98	251.6
12	4.69	6.70	83	241	0.28	240.9
13	5.72	6.65	81	225	1.03	225.5
14	6.67	6.61	87	230	0.95	229.7
15	5.78	6.28	92	231	0.95	230.9
16	5.56	6.29	90	230	0.22	229.8
17	5.32	6.19	84	230	0.27	229.6
18	4.67	6.32	73	234	0.65	234.3
19	5.64	5.52	75	227	1.25	227.1
20	7.52	5.19	77	207	1.91	206.5
21	7.29	5.38	88	222	0.29	222.1
22	7.12	5.26	82	194	0.21	193.7
23	7.38	5.34	83	222	0.27	222.2
24	7.66	4.41	83	214	0.97	213.8
25	7.71	3.82	90	221	0.59	220.8

Figure 1.4. An example of spot tracker result.

Using spot tracker data, many quantitative results can be achieved. Firstly, when spot position (x) versus spot position (y) is plotted, trajectories of quantum dots in live cells can be determined. Using these trajectories, type of diffusion for quantum dots in cellular environment can be achieved.

Moreover, using x spot and y spot data, mean square displacement (MSD) of quantum dots can be determined. When MSD versus time plot is drawn, diffusion coefficients can be calculated from the slope of the MSD plot. Intensity change of quantum dots in the course of time is another result that can be determined using ImageJ data. This will be useful in order to understand whether photobleaching occurs or not.

CHAPTER 2

SYNTHESIS AND PHYSICOCHEMICAL CHARACTERIZATION OF CdS_xSe_{1-x} QUANTUM DOTS

2.1. Introduction

Nanobiotechnology is advanced in recent years by incorporation of nanomaterials with biomaterials. Among various nanomaterials, quantum dots (QDs) attracted much attention in nanobiotechnology. In a few words, quantum dots are luminescent nanocrystals. Developments in nanocrystal technology came into sight in the early 1980s by Alexander Efros, Alexie Ekimov (Yoffe Institute, Russia) and Louis Brus (Bell Laboratories, USA). They studied with nanocrystal semiconductor materials and observed different colors from the same substance. This work contributed to the understanding of the correlation between size and color for these nanocrystals. After that Moungi Bawendi and Paul Alivisatos continued investigating and improving optical properties of quantum dots (Borrelli 2003).

Quantum dots are colloidal semiconductor nanocrystals. They are generally composed of atoms from groups II and VI or III and V of the periodic table such as CdS, CdSe, CdTe, etc. Characteristic size of quantum dots ranges from 2 nm to 20 nm (Kluson et al. 2007), but according to another literature cadmium based binary materials have diameter lower than 10 nm (Kral et al. 2006). When their diameter is larger than 10 nm, they become bulk material and do not exhibit quantum confinement behaviour. A system must show quantum confinement effect to be called quantum dot. Quantum confinement arises from the geometric confinement of holes and electrons known as excitons. The normal size of an exciton in a bulk crystal (exciton Bohr radius) provides an approximate dimension for the onset of quantum confinement effects. When an electron–hole pair is squeezed into a nanocrystal with one or more dimensions approaching the bulk exciton Bohr radius, an increase in the effective bandgap of the semiconductor is observed. The smaller the nanocrystal, the larger the effective bandgap, so the greater the energy of optical emission resulting from electron–hole

recombination. Typical exciton Bohr radii range from 11 nm (InP) to 60 nm (InSb) in III–V semiconductors, and from 2.2 nm (ZnS) to 7.5 nm (CdTe) in II–VI semiconductors. Magnitude of quantum confinement depends on size, composition and shape of nanocrystal. Quantum wells are confined in one dimension, quantum wires are confined in two dimension and quantum dots are confined in three dimension (Buhro and Colvin 2003).

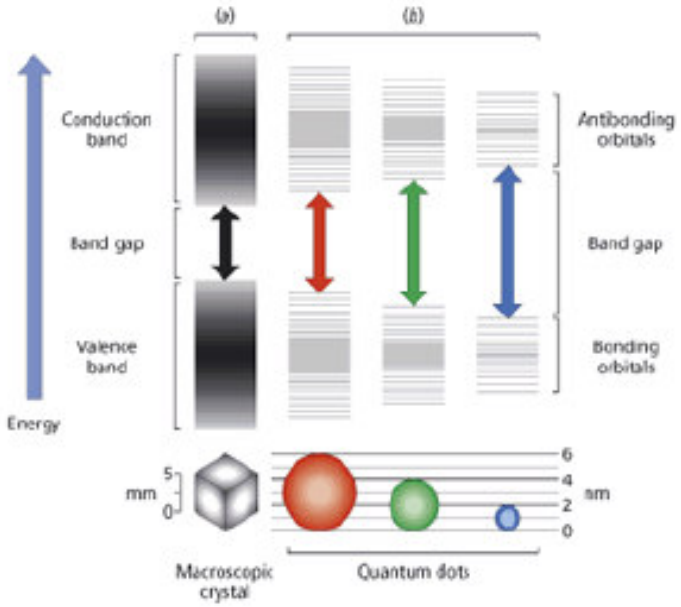

Figure 2.1. Schematic representation of band offsets of quantum dots.
(Source: Evidenttech 2009)

As a result of quantum confinement effect, these tiny particles gain characteristic electronic and optical properties which make them advantageous over current fluorophores, such as fluorescent proteins and organic dyes. QDs have broad absorption spectra which make it possible to be excited by a wide range of wavelengths. As a result, different colored quantum dots can be excited using a single wavelength. Moreover, quantum dots have narrow emission spectra which can be tuned by altering size, composition and surface chemistry of quantum dots (Jamieson et al. 2007). They emit light from ultraviolet (UV) to infrared (IR) region. Quantum dots have very high surface to volume ratio, high quantum yield, narrow full width at half maximum (FWHM), large molar extinction coefficient and large Stoke's shift. Another advantage of quantum dots is that they have long fluorescence lifetime and high resistivity to

photobleaching. These properties make quantum dots superior to organic dyes in detection sensitivity as well as in long term tracking of biological process.

Among various quantum dots, CdX (X=S, Se, Te) are the most examined quantum dots because of wide availability of precursors, size-tunable fluorescence from UV-Vis to NIR regions and well defined crystal growth (Biju, Itoh, and Ishikawa 2010). However these are core quantum dots and their emission ability and stability are strongly affected by the surface because of high surface area to volume ratio and also the presence of surface traps arising from unsaturated bonds, surface stoichiometry and surface traps (Gu et al. 2008). At that point, surface passivation of quantum dots with a suitable material is necessary. Capping core nanocrystals with a higher band gap semiconductor generates core/shell quantum dots. Shell plays an important role, it should be structurally similar to core material to confine the excitation to core effectively. Formation of a shell around core creates a quantum dot with improved luminescence, higher stability and quantum yield (Jamieson et al. 2007).

Alloying of two semiconductor produces materials whose properties are different from both core and shell materials. As a result, alloy nanocrystals have extra properties that are composition dependent apart from the properties resulting as a result of quantum confinement effects (Regulacio and Han 2010).

Alloy quantum dots can be grouped into two categories according to composition: homogeneous alloys, having uniform internal structure and gradient alloys, having different composition in different parts of the alloys. Depending on number of elements in the alloy, quantum dots can be either ternary (three elements) or quaternary (four elements). Ternary alloys are formed when the parents are two binary systems whether with a common anion or cation. As an example, alloying of AE and BE produces $A_xB_{1-x}E$. Here A and B are different cations, E is common anion.
e.g. $Zn_xCd_{1-x}Se$ is a common anion alloy of ZnSe and CdSe. In order to form common cation alloy, AE_xF_{1-x} , AE and AF can be used where A is common cation, E and F are different anions. e.g. CdS_xSe_{1-x} is a common cation alloy of CdS and CdSe.

Unfortunately, most of the quantum dots are toxic. Cadmium ions are the primary cause of cytotoxicity, because of the fact that they can bind to thiol groups on molecules in mitochondria. However, it is possible to reduce or eliminate release of Cd^{2+} by addition of further surface coating (Drbohlavova et al. 2009). Another drawback of quantum dots is that they are generally non-dispersible in water which is

caused by the use of organic solvents so by the presence of hydrophobic molecules. However, there are effective methods to make these quantum dots soluble including ligand exchange, silica encapsulation and hydrophobic interaction.

In our study, we synthesized TOPO capped CdS_xSe_{1-x} quantum dots using a modified two phase synthesis method (Pan et al. 2005) and synthesized quantum dots are estimeted to have a gradient structure because of different reaction rates of S and Se. However, it was necessary to make CdS_xSe_{1-x} dispersed in water for live cellular imaging studies. For this purpose, ligand exchange method was applied.

2.2. Experimental

2.2.1. Synthesis of CdS_xSe_{1-x} Quantum Dots

2.2.1.1. Preparation of Se Precursor (NaHSe)

NaHSe solution was prepared by reacting sodium borohydrate ($NaBH_4$) with selenium powder in a reaction flask, under nitrogen atmosphere, at room temperature. $NaBH_4$ reduces the charge of selenide from 0 to -2. The reaction is considered to be as below:

$$4NaBH_{4(aq)} + 2Se_{(s)} \rightarrow 2NaHSe_{(aq)} + Na_2B_4O_{7(s)} + 14H_{2(g)} \quad (2.1)$$

Ultra pure water was then added to the reaction flask. A clear NaHSe solution was obtained with a white precipitate, $Na_2B_4O_7$, at the bottom of the reaction flask. NaHSe is very sensitive to air, it can be oxidized easily so in all experiments freshly synthesized NaHSe solution was used without any purification.

2.2.1.2. Preparation of CdS_xSe_{1-x} Quantum Dots

A modified literature method was adopted in order to synthesize CdS_xSe_{1-x} quantum dots by two phase method (Pan et al. 2005). Firstly, cadmium oxide and myristic acid were reacted at 250ºC to form cadmium myristate. Cadmium myristate

and trioctylphosphine oxide (TOPO, as capping agent, shown in Figure 2.3) were dissolved in toluene at 80ºC. In a two-neck round-bottom flask, thiourea (S source, shown in Figure 2.4) was dissolved in ultra pure water, at 100ºC, under nitrogen atmosphere. Then, NaHSe was added to aqueous thiourea solution by the help of a syringe. New solution was stirred vigorously. Next, readily prepared toluene solution was introduced to reaction medium, a solution with two different phases formed, water phase was at the bottom while toluene phase was at the top of the mixture. CdS_xSe_{1-x} quantum dots are estimated to grow at the toluene-water interface (Pan et al. 2007).

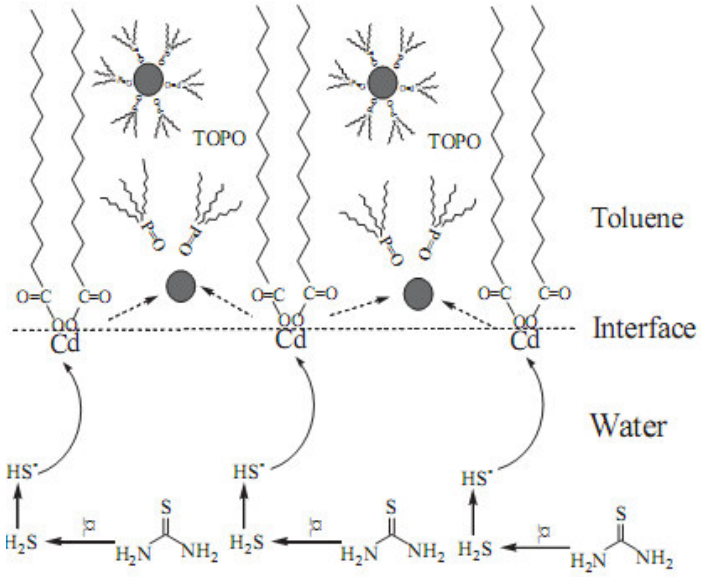

Figure 2.2. A proposed mechanism for formation of CdSe in oil phase.
(Source: Pan et al. 2007)

Nearly, after 30 minutes, alloy CdS_xSe_{1-x} quantum dots started to grow. Aliquots of sample were taken from the reaction flask, at different time intervals to monitor growth of nanocrystals in the course of time. Aliquots were characterized by UV-Vis absorption and fluorescence spectroscopies. Until the desired wavelength was achieved, the reaction was proceeded. The growth of nanocrystals can be stopped by cooling the solution to the room temperature.

Once synthesized, CdS_xSe_{1-x} quantum dots were isolated by applying precipitation with ethyl alcohol in centrifuge. Precipitation was applied several times to remove excess capping agent (TOPO) and also impurities. Precipitated CdS_xSe_{1-x}

quantum dots were left to dry at room temperature. After being dried, they were stored in a vial which is saturated with nitrogen gas, in a refrigerator.

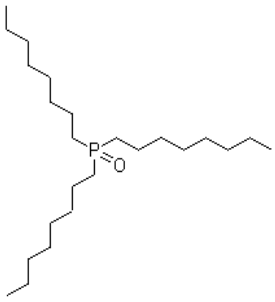

Figure 2.3. Structure of TOPO.

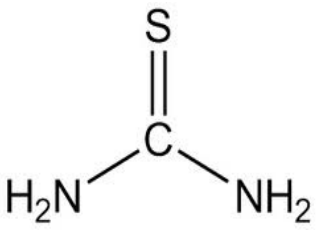

Figure 2.4. Structure of thiourea.

2.2.2. Ligand Exchange for CdS_xSe_{1-x} Quantum Dots

Synthesized TOPO capped CdS_xSe_{1-x} quantum dots were dispersed in toluene therefore they are not water dispersible. They have to be made water dispersible to be useful for cellular imaging studies. It is possible to make these quantum dots water dispersible by applying ligand exchange method. For that purpose, it was aimed to exchange TOPO with 3-mercaptopropionic acid (3-MPA, shown in Figure 2.5) and N-Acetyl-L-Cysteine (NAC, shown in Figure 2.6) which are soluble in water. A method from literature was modified to exchange capping agent around CdS_xSe_{1-x} quantum dots (Zhang et al. 2008).

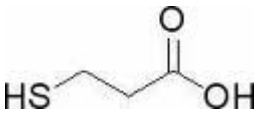

Figure 2.5. Structure of 3-MPA.

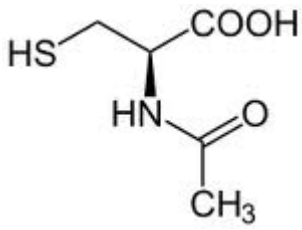

Figure 2.6. Structure of NAC.

Firstly, TOPO capped CdS_xSe_{1-x} quantum dots were dispersed in chloroform. Then, MPA/NAC were added to ultra pure water and pH of the solution was adjusted to 10.0 with 1.0 M NaOH. These two solutions were mixed in a falcon tube. Two different phases were observed: Lower phase (green) contained quantum dots in chloroform

whereas upper phase (transparent) contained MPA/NAC in ultra pure water. The solutions were mixed for twenty four hours at room temperature At the end of twenty four hours, it was observed that water phase was green indicating the transfer of quantum dots from chloroform to water. Two phases were seperated and particles were obtained as solid after applying precipitation to water phase using ethyl alcohol.

2.3. Results & Discussion

2.3.1. Optical Characterization

Ultraviolet-visible absorption and fluorescence emission spectroscopies are used for optical characterization of quantum dots.

Absorption of visible and UV radiation are associated with excitation of electrons in atoms and molecules to higher energy levels. Absorbance is just a measure of the amount of light absorbed. The higher the value, the more of a particular wavelength is being absorbed. The wavelength of light that a compound will absorb is characteristic of its chemical structure.

Fluorescence is a spectrochemical method of analysis where the molecules of the analyte are excited by irradiation at a certain wavelength and emit radiation of a different wavelength. The emission spectrum provides qualitative and quantitative information.

Optical characterization of synthesized CdS_xSe_{1-x} quantum dots was performed by using ultraviolet-visible absorption and fluorescence spectroscopies which offer fast, non destructive and contactless option (Drbohlavova et al. 2009).

UV-Visible absorption spectra were recorded on a Varian Cary 50 UV-Vis Spectrometer. Aliquots from reaction flask were taken at different times and their UV-Vis spectra were recorded to observe growth of quantum dots in the course of time.

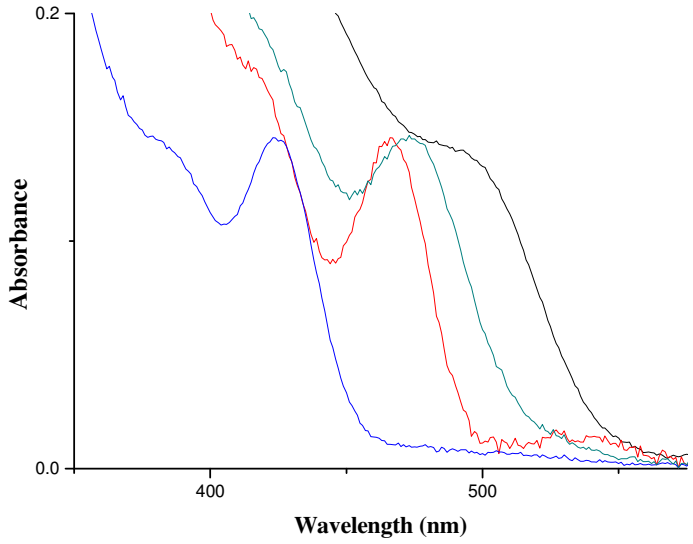

Figure 2.7. UV-Vis spectra of CdS_xSe_{1-x} quantum dots.

Figure 2.7 shows the UV-Vis absorption spectra of the resulting CdS_xSe_{1-x} quantum dots. Growth of nanocrystals started after thirty minutes and continued for six hours. At the beginning of the reaction, absorption wavelength was 430 nm whereas at the end of the reaction absorption wavelength was 495 nm. On prolonging the reaction time, spectra shifted to longer wavelength indicating the increase in size of CdS_xSe_{1-x} quantum dots. Size of nanoparticles can be calculated from UV-Vis spectra using the Equation 2.2 (Ethayaraja et al. 2007).

$$E_g = E_{gb} + \frac{h^2}{2d^2}\left(\frac{1}{m_e} + \frac{1}{m_h}\right) - \frac{3.6e^2}{4\pi\varepsilon d} \tag{2.2}$$

Bulk band gap (E_{gb}) is 1.73 eV, effective electron mass (m_e) is 0.11 m_0, effective hole mass (m_h) is 0.45 m_0, dielectric constant (ϵ) is 9.6 ϵ_0 for CdSe quantum dot. As well, h is Planck's constant, d is diameter of nanoparticle, e is the electronic charge (Joshi et al. 2006). When these values are inserted into equation above, Equation 2.3 is obtained:

$$\frac{1}{d} = 0.0089 + \sqrt{\frac{38.56}{\lambda} - 0.057} \tag{2.3}$$

where λ is the first exciton peak cutting through wavelength axis in absorption spectrum and d is diameter of nanoparticle. Size of the quantum dots was calculated using the Equation 2.2 and it was proved that their size increased in the course of time from 3.1 nm to 4.3 nm.

Fluorescence spectra were taken on a Varian Cary Eclipse Fluorescence Spectrometer. Aliquots from reaction flask were taken at different times and their fluorescence spectra were recorded to observe growth of quantum dots in the course of time. In Figure 2.8, fluorescence spectra of the resulting CdS_xSe_{1-x} quantum dots are seen. Fluorescence spectra span from 400 nm to 600 nm. At the beginning of the reaction, fluorescence wavelength was 450 nm and it reached to 530 nm at the end of the experiment. A shift to longer wavelength is an indication of increase in particle size.

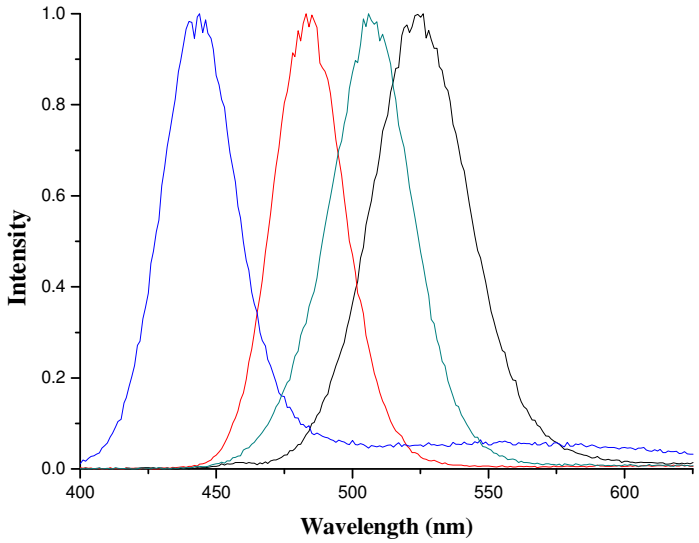

Figure 2.8. Fluorescence spectra of CdS_xSe_{1-x} quantum dots.

In Figure 2.9, the growth kinetics of CdS_xSe_{1-x} quantum dots is shown. As seen from the Figure 2.9, particle growth depends on time. In the first two hours, particle growth was quick however, growth of particles slowed down as time passing. Because it takes more time for capping agent to cover the surface of particles.

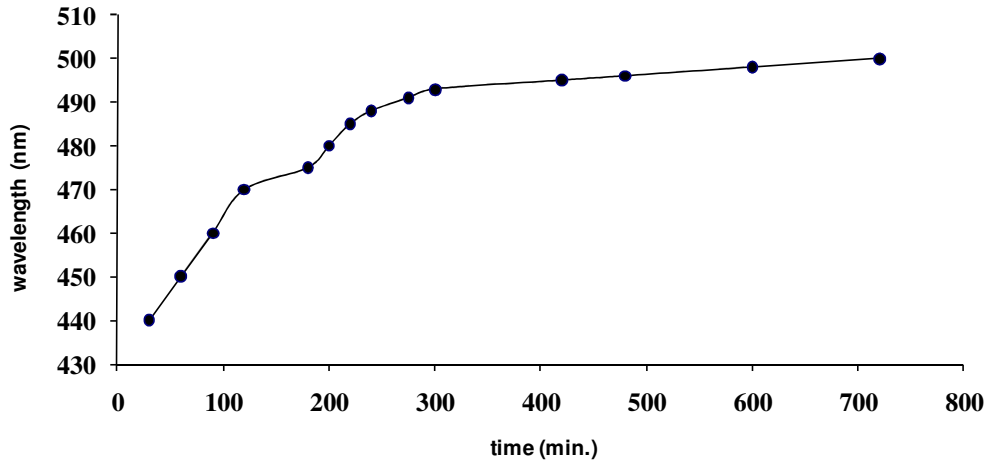

Figure 2.9. Temporal evolution of fluorescence peaks of CdS_xSe_{1-x} quantum dots.

Quantum yield (QY) of synthesized CdS_xSe_{1-x} quantum dots was calculated by using Rhodamine 6G as reference, using the Equation 2.4:

$$\Phi = \Phi_R \frac{Int}{Int_R} \frac{A_R}{A} \frac{n^2}{n_R^2} \quad (2.4)$$

In this equation, Φ is the quantum yield, *Int* is the area under the emission peak, *A* is absorbance at the excitation wavelength, and n is the refractive index of the sample. Φ_R, A_R and n_R are quantum yield, absorbance at the excitation wavelength and refractive index of reference respectively. QY of synthesized CdS_xSe_{1-x} quantum dots was between 80-85%.

2.3.2. Structural Characterization

X-ray diffraction (XRD) spectroscopy, infrared (IR) spectroscopy and dynamic light scattering (DLS) measurements are indispensible structural characterization methods.

X-ray diffraction analysis is a rapid and nondestructive analytical method to investigate the crystal structure, chemical composition and size. The sample is irradiated with monochromatic X-ray light and the stray radiation is recorded. X-ray diffraction

analysis uses the property of crystal lattices to diffract monochromatic X-ray light. The diffraction pattern for every phase is as unique as fingerprint (Pecharsky 2008).

Dynamic light scattering (DLS) technique is one of the most widely used methods in order to determine size of particles. Shining a monochromatic light beam on a solution, in which spherical particles undergo Brownian motion, causes Doppler Shift when the light strikes the moving particle, altering the wavelength of the incoming light. This change is directly proportional to size of the particle.

IR spectroscopy is one of the most common spectroscopic techniques in order to determine functional groups in molecules. Simply, it is the absorption measurement of different IR frequencies by a sample positioned in the path of an IR beam. Different functional groups absorb different frequencies of IR radiation. Significant points for the identification of the source of an absorption band are intensity (weak, medium, strong), shape (broad, sharp) and position (cm^{-1}) in the spectrum.

Structural characterization of synthesized CdS_xSe_{1-x} quantum dots was performed by using X-Ray Diffraction (XRD), Infrared (IR) Spectroscopy and Dynamic Ligth Scattering (DLS) techniques.

In order to find crystal structure of nanocrystals, hkl indices of peaks in the XRD diffractogram should be determined using Bragg's Law shown in equation below:

$$n\lambda = 2d \sin\theta \tag{2.5}$$

where n is the order, λ is the wavelength of X-rays and d is the interplanar spacing between planes in the atomic lattices and θ is the angle between incident beam and scattering beam. In Figure 2.10, XRD pattern of green emitting TOPO capped CdS_xSe_{1-x} quantum dots is displayed. This diffractogram was used to determine the structure of quantum dots. By comparing hkl indices of bulk CdS and CdSe, crystal structure of CdS_xSe_{1-x} quantum dots was estimated to be face centered cubic (Pan et al. 2007).

In order to find crystal size, Debye Scherrer's equation can be applied to XRD pattern

$$D = 0.9\lambda/\beta \cos\theta \tag{2.6}$$

where D is the diameter of the crystals, λ is the wavelength of the incident X-rays, β is the full width at half maximumof the Bragg's peak and θ is the diffraction angle. From Debye Scherrer's equation, the size of quantum dots were found to be 3.0 nm.

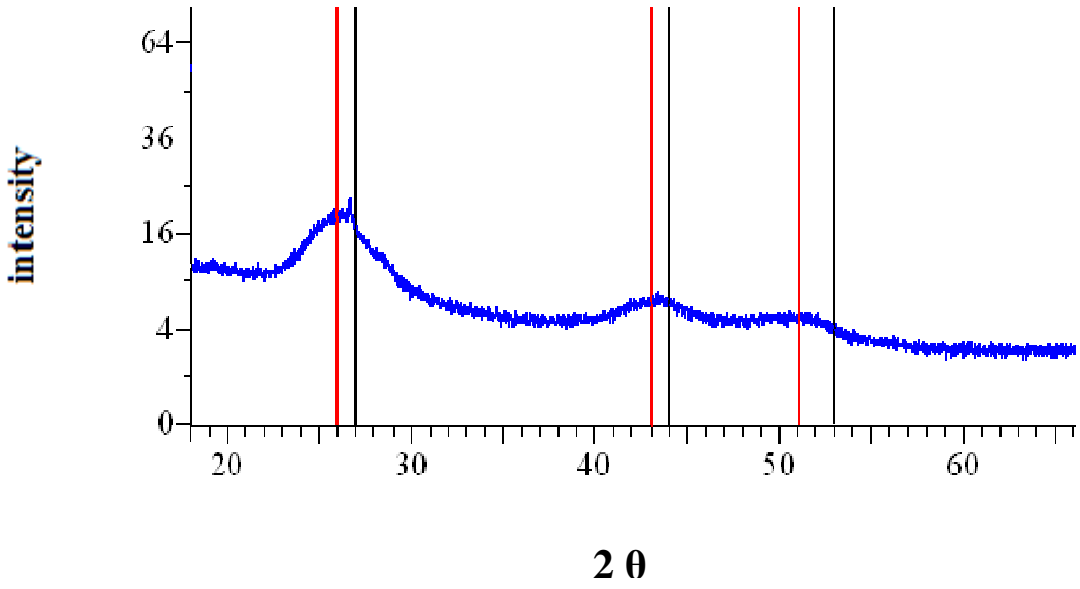

Figure 2.10. XRD spectra of green emitting TOPO capped CdS_xSe_{1-x} quantum dots.
red lines: hlk indices of cubic bulk CdSe (111,220,311 respectively)
black lines: hlk indices of cubic bulk CdS (111,220,311 respectively)

Dynamic light scattering (DLS) is a powerful technique to determine size and also size distribution profile of small particles in suspension. In Figure 2.11 DLS analysis of TOPO capped CdS_xSe_{1-x} quantum dots is shown. Hydrodynamic diameter (size) of quantum dots were 5.2 nm. It is apparent that size of quantum dots according to DLS result (5.2nm) is bigger than that of quantum dots according to XRD result (3.0 nm). DLS measures hydrodynamic diameter of quantum dots, however, XRD measures the crystal size. In XRD result, size of hydration layer of water molecules around quantum dots is not included because XRD detects only the crystal part of the molecule.

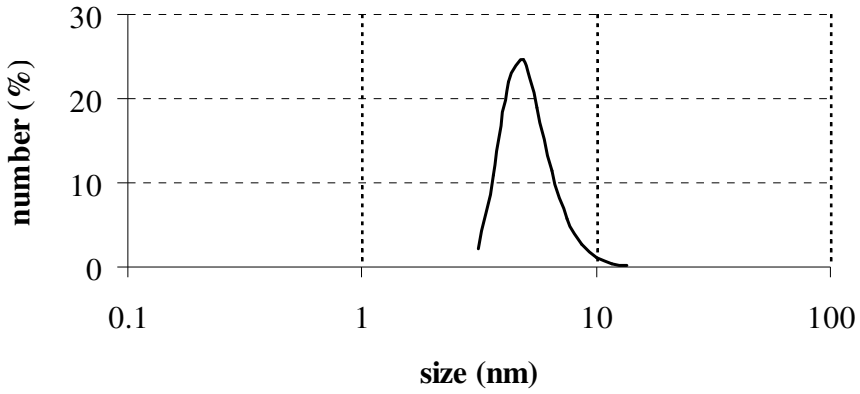

Figure 2.11. DLS analysis of TOPO capped green emitting CdS_xSe_{1-x} quantum dots.

After exchanging TOPO molecules around CdS_xSe_{1-x} quantum dots with MPA and NAC molecules, there was not a notable change in the size of quantum dots. As it is seen from the Figure 2.12, MPA capped CdS_xSe_{1-x} quantum dots have a diameter of 5.8 nm. Figure 2.13 shows that NAC capped CdS_xSe_{1-x} quantum dots are 8.9 nm in size.

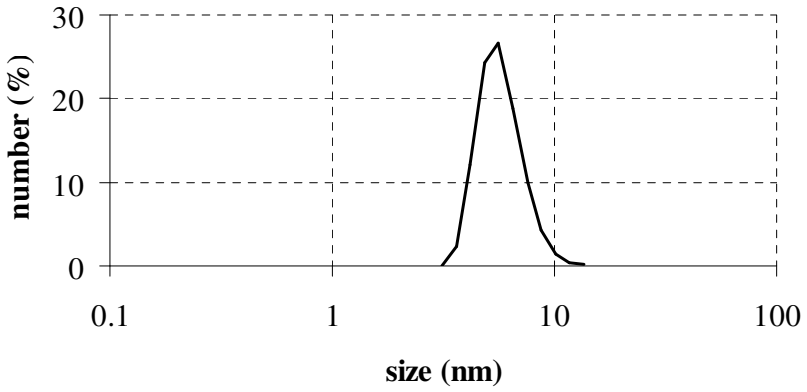

Figure 2.12. DLS analysis of MPA capped green emitting CdS_xSe_{1-x} quantum dots.

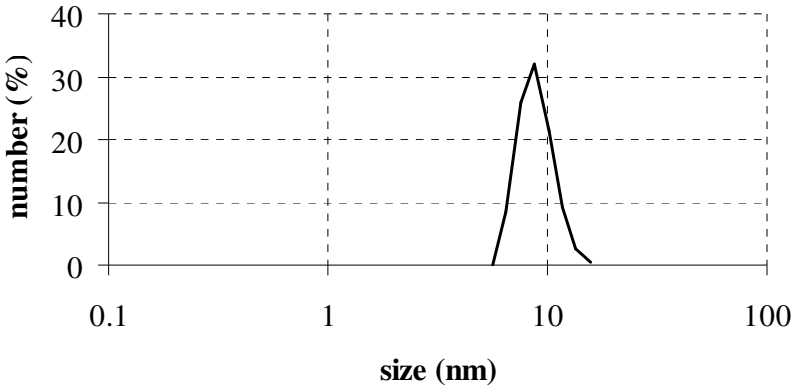

Figure 2.13. DLS analysis of NAC capped green emitting CdS_xSe_{1-x} quantum dots.

Infrared spectroscopy was used to determine the functional groups in molecules. In Figure 2.14, FTIR spectrum of TOPO capped CdS_xSe_{1-x} quantum dots is seen. The sharp peak at 1400 cm^{-1} arises from C-C and the peak at 900 cm^{-1} is for C-H in TOPO. The signals between 1100 and 1200 cm^{-1} indicaes the presence of P=O in TOPO.

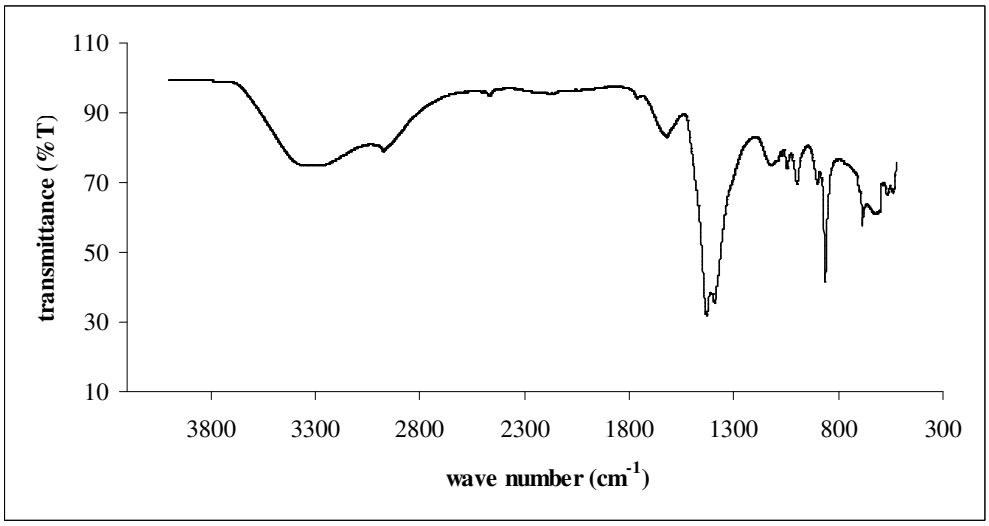

Figure 2.14. FTIR spectrum of green emitting TOPO capped CdS_xSe_{1-x} quantum dots.

Figure 2.15 shows the IR spectrum of green emitting MPA capped CdS_xSe_{1-x} quantum dots. In the spectrum, the absorption band at 1700 cm^{-1} is very sharp which is characteristic of C=O for carboxylic acid derivatives. Moreover, the bands between 1000-1250 cm^{-1} indicates the presence of C-N.

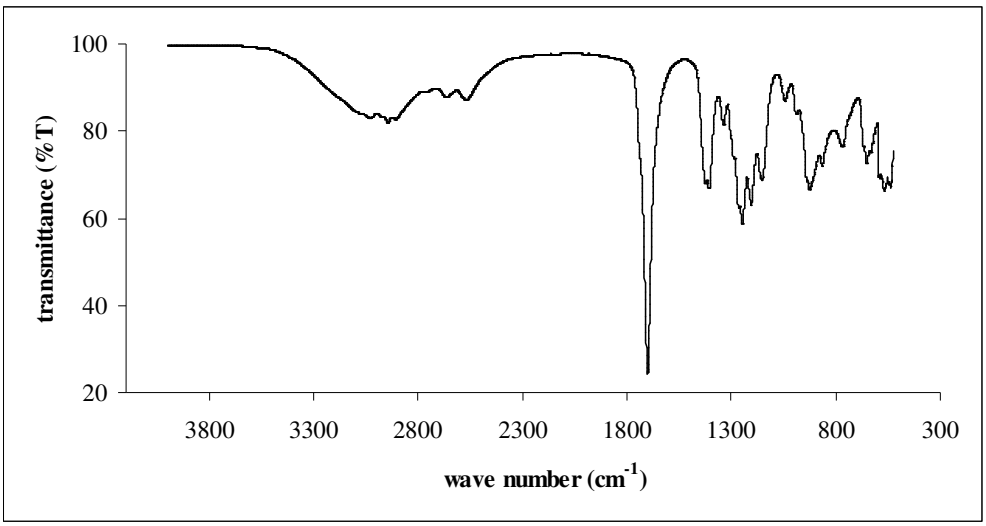

Figure 2.15. FTIR spectra of green emitting MPA capped CdS_xSe_{1-x} quantum dots.

Figure 2.16 shows the FTIR spectrum of green emitting NAC capped CdS_xSe_{1-x} quantum dots. The absorption peak at 2600 cm^{-1} is for S-H group and also the peak at 3400 cm^{-1} implies the presence of N-H.

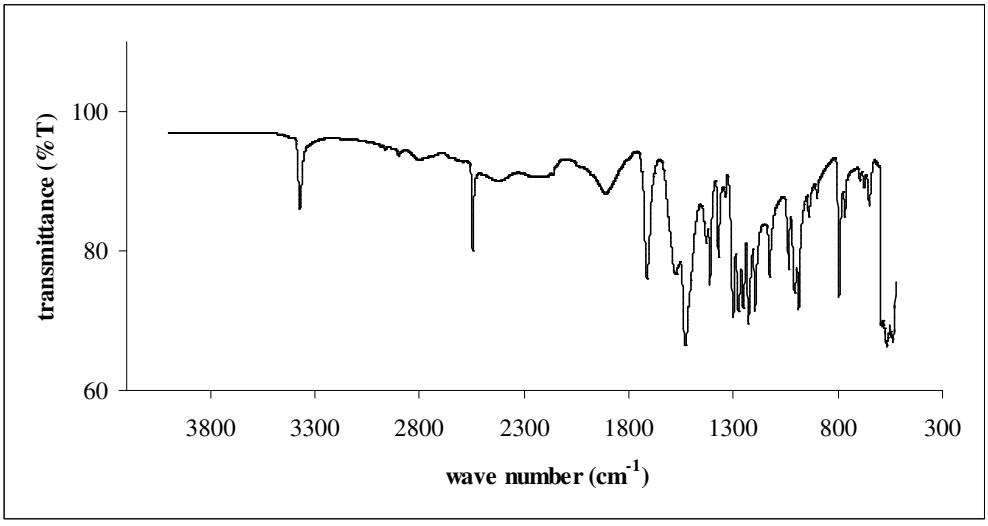

Figure 2.16. FTIR spectra of green emitting NAC capped CdS_xSe_{1-x} quantum dots.

2.4. Conclusion

Highly luminescent TOPO capped CdS_xSe_{1-x} quantum dots were synthesized by the two phase synthesis method. Crystal structure of synthesized quantum dots was estimated to be face centered cubic. Hydrodynamic radius of CdS_xSe_{1-x} quantum dots varied from 5 nm to 9 nm. The fluorescence wavelength of quantum dots was set to 520 nm in order to make them matched for emission filter of confocal microscope. Surface modification was carried out to replace TOPO by MPA and NAC in order to make quantum dots water dispersible for cellular imaging studies. After surface modification, fluorescence quantum yield decreased to 20% from 80 %. In Table 2.1 photophysical properties of TOPO capped CdS_xSe_{1-x} quantum dots is seen. In the course of time Stokes shift, FWHM, QY and of QDs increase.

Table 2.1. Photophysical Properties of TOPO Capped CdS_xSe_{1-x} QDs

Sample Name	$\lambda_{absorption}$ (nm)	$\lambda_{fluorescence}$ (nm)	Stokes Shift (nm)	FWHM (nm)	QY (%)	Size (nm)
CdS_xSe_{1-x} 1	423	445	22	29	45	3.5
CdS_xSe_{1-x} 2	466	485	19	30	75	4.5
CdS_xSe_{1-x} 3	476	505	29	36	80	5.0
CdS_xSe_{1-x} 4	495	525	30	40	80	5.2

CHAPTER 3

TRACKING REAL TIME MOTIONS OF CdS_xSe_{1-x} QUANTUM DOTS IN LIVE CELLS

3.1. Introduction

The use of quantum dots in bioimaging is the most widely preferred application of quantum dots. It is necessary to determine locations, mobilities and uptake mechanisms of quantum dots. Many factors influence intracellular pathways and localization of quantum dots in cells. The most important physicochemical parameters are, charge, size and surface coating of quantum dots.

The first thing to be considered is the location of quantum dots in cells. Many nanomaterials are observed to be localized in cells. Fullerenes have been localized in human fibroblasts (Sayes et al. 2004). Coated magnetite nanoparticles were observed in human mammary carcinoma cells (Zhang et al. 2002). Carbon nanotubes have been localized in human epidermal keratinocytes (HEK). CdSe quantum dots were coated with trimethoxysilylpropyl urea and acetate groups were found to bind to nucleus of the 3T3 mouse fibroblast cells (Bruchez et al. 1998). CdSe/ZnS-PEG-COOH quantum dots were incubated with NIH3T3 (mouse embriyonic fibroblast cell line) and MCF-7 (human breast adenocarcinoma cell line). It was observed that there was no quantum dot inside the nucleus of any cell but in NIH3T3 cells quantum dots were observed through the golgi complex in the perinuclear region (Damalakiene, Bagdonas, and Rotomskis 2009). Vibin and coworkers reported that silica coated CdSe quantum dots were localized in the intracellular vesicles causing strong fluorescence from the cytoplasm and nearby nucleus (Vibin et al. 2011). In another study, CdSe/ZnS core shell quantum dots were successfully incorporated to human cervical cancer cells (HeLa) and they were internalized into cytoplasm of HEK. (Zhang and Monteiro-Riviere 2009). Damalakiene and coworkers' observed quantum dots to end up in intracellular vesicles that could be identified as endosomes or lysosomes or in a perinuclear region

compatible with endosomal/lysosomal localization (Damalakiene, Bagdonas, and Rotomskis 2009).

The second thing to be considered is uptake mechanisms of quantum dots to cells. Labeling of cells using bioconjugated quantum dots can be classified into two categories: nonspecific and targeted.

Nonspecific extracellular binding of quantum dots to cell membrane is a result of hydrophobic and electrostatic interactions between biomolecules in the cell membrane and capping molecules on the surface of the quantum dot. The amount of adsorption of quantum dots to cell membrane is directly proportional to size of quantum dots on account of the fact that larger quantum dots have more ligands which cause electrostatic interactions with cell membrane (Biju, Itoh, and Ishikawa 2010).

Nonspecific intracellular delivery of quantum dots takes place by applied methods (micro/nano injection, osmotic lysis, electroporation) and by adopted methods by cells (Steinman et al. 1983). Adopted methods follow the general way of endocytosis. Endocytosis is a process in which a substance gains entry into a cell without passing through the cell membrane. This process is subdivided into three different types: pinocytosis, phagocytosis and receptor mediated endocytosis (Alberts et al. 2002). In each case, an intracellular vesicle forms by virtue of the invagination of the plasma membrane and membrane fusion. The different categories differ in the exact mechanisms by which this process occurs.

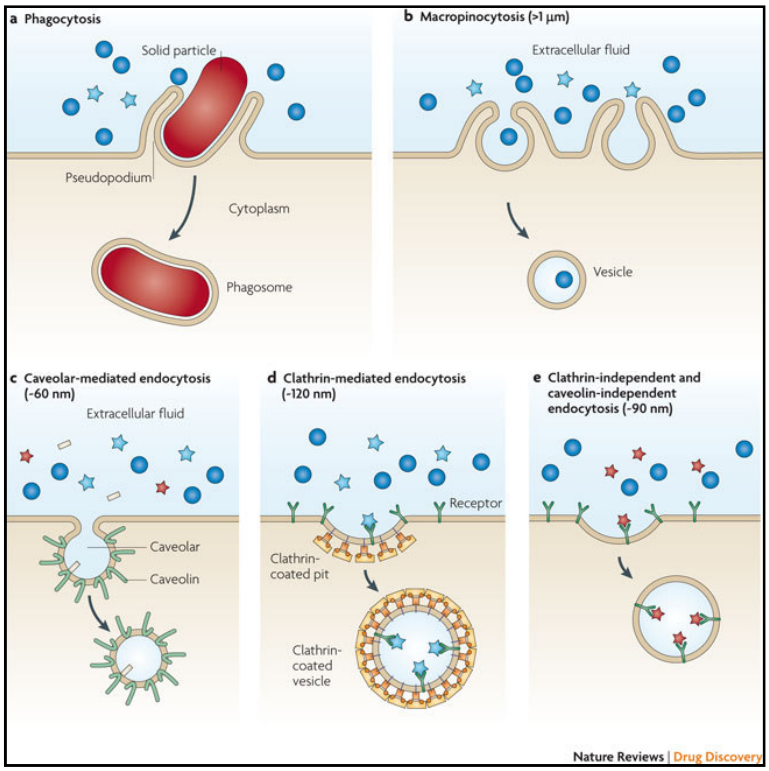

Figure 3.1. Modes of cellular internalization of nanoparticles and respective size limitations. Nanoparticles are represented by blue circles (> 1 μm), blue stars (about 120 nm), red stars (aout 90 nm) and yellow rods (about 60 nm). (Source: Petros et al. 2010)

Clathrin-mediated endocytosis is common for all cell types (Biju et al. 2010). In this type of endocytosis, foreign molecules (nanoparticles and biomolecules) attach to proteins or membrane receptors and then they get trapped along with clustered receptors into approximately 100 nm size clathrin-coated pairs.

In caveolae-dependent endocytosis, biomolecules or nanoparticles are trapped into 50 nm sized small caves formed by lipid-raft invaginations in the cell membrane (Biju et al. 2010).

Nonspecific endocytosis neither limits the intracellular delivery of quantum dots in a particular type of cell nor facilitates targeting of a particular organelle or molecule in cells because it is not mediated by any target molecule (Biju et al. 2010). Therefore, nonspecific endocytosis of quantum dots is significant in the extended imaging of cell samples and investigation of endocytosis mechanism.

The third thing to be considered is intracellular diffusion pathways of quantum dots in cells. Diffusion is a principle way of movement of substances in cells, as well as the method for essential small molecules to cross through the cell membrane. In order to

understand the type of diffusion and also to calculate diffusion coefficient, mean square displacement (MSD) versus time graph can be plotted. MSD is a measure of average distance a molecule travels. Kusumi and coworkers reported that five types of motion were observed for molecules in cells and motions were characterized depending on MSD versus time plots (Kusumi, Sako, and Yamamoto 1993).

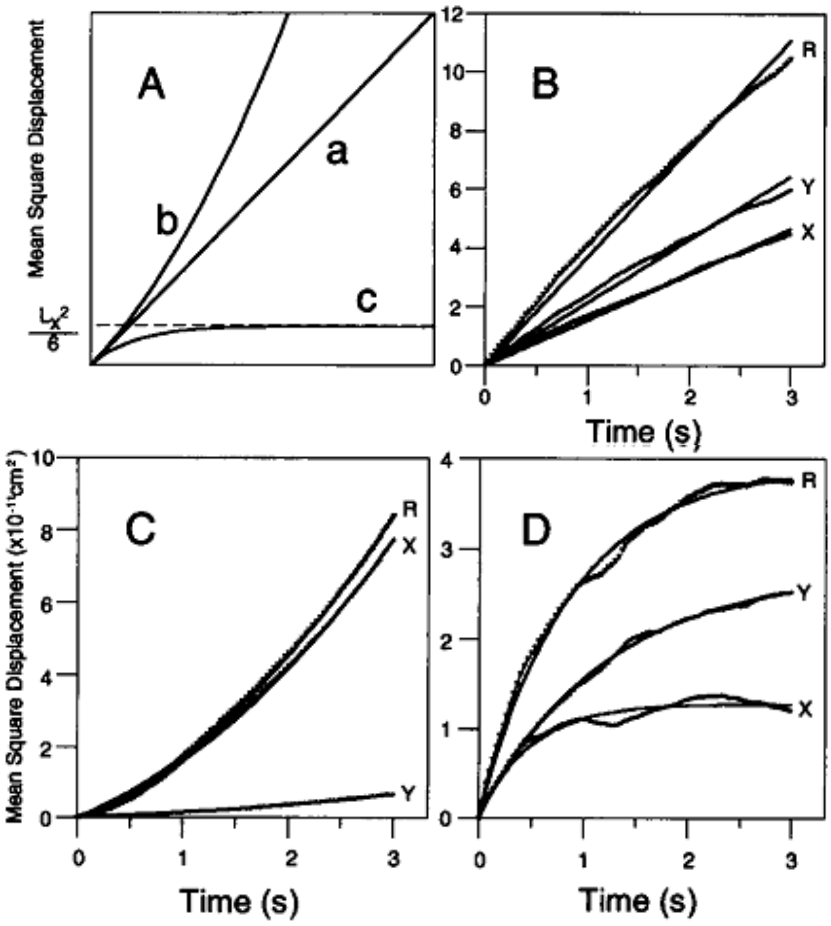

Figure 3.2. MSD-Δt plots for diffusing particles. (A) simple Brownian diffusion(a), directed diffusion(b), restricted diffusion(c) in one dimension. (B) simple diffusion (C) directed diffusion (D) restricted diffusion. X, Y, R indicate diffusion in the x and y directions and in a two dimensional plane, respectively. (Source: Kusumi et al. 1993)

Stationary diffusion: Diffusion coefficient (D) < 4.6 x 10^{-12} cm^2/s are classified in this category.

Simple diffusion: In this type of diffusion, molecules undergo simple Brownian motion. MSD versus time plot is linear and its slope is 4D.

Directed diffusion: Molecules move with a constant velocity and MSD plot is parabolic.

Restricted diffusion: Molecules perform Brownian diffusion within a limited region and they are unable to move out of this area during observation period (Kusumi, Sako, and Yamamoto 1993).

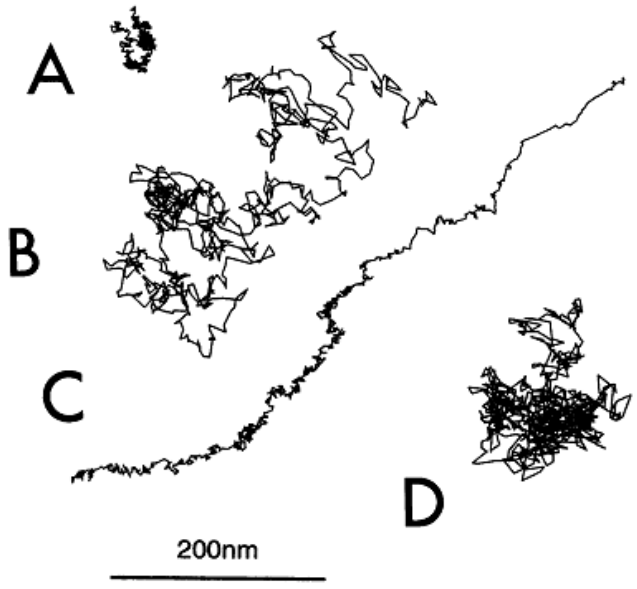

Figure 3.3. Typical trajectories of particles (A) stationary mode (B) simple diffusion mode (C) directed diffusion mode (D) restricted diffusion mode.
(Source: Kusumi et al. 1993)

After determination of localization, uptake mechanisms, diffusion pathways and mobilities of quantum dots in cells, it would be meaningful to use them for biological applications.

3.2. Experimental

3.2.1. Cell Culture Studies

Two types of cell lines were used: A cancer cell line, A549 (Human lung adenocarcinoma epithelial cell line) and a healthy cell line, BEAS 2B (Human bronchial

epithelial cell line). A549 and BEAS 2B cell lines were kindly provided by Professor Hasan Bayram (Gaziantep University, Medical Faculty). A549 cell line grew in Dulbecco's Modified Eagle Medium (DMEM) and BEAS 2B cell line grew in Roswell Park Memorial Institute 1640 medium (RPMI). Media were supplemented with 10% fetal bovine serum (FBS), 1% Penicillin–Streptomycin as antibiotic and. 1% L-Glutamine as amino acid. Both cell lines were maintained in a dark cell incubator having 5% carbondioxide (CO_2) and 95% humidity at 37ºC.

Cells were grown in flasks. When the available substrate surface is covered by cells (a confluent culture) growth slows down and ceases. When confluency reached to 80-85%, cells were sub-cultured or passaged to be kept in healthy and growing state. Firstly, the culture medium was removed from subconfluent flasks, cells were rinsed twice with steril phosphate buffer solution (PBS). Then, the cells were incubated with trypsin/EDTA for five minutes in a dark cell incubator at 37ºC. Cell culture media has trypsin neutralizers, so when cells were washed with PBS beforehand these factors were washed away, making trypsin active. Trypsinized cells were transferred into centrifuge cells at 3000 round per minute (rpm) for three minutes. Formed pellet was resuspended in cell culture medium and cells were counted using a hemocytometer. Cells were seeded to flask and allowed to grow in incubator. When the passage number reached to fifteen, cells were disposed off and new cells were started to be used (Masters 2000).

For imaging studies, the cells were seeded to µ-dishes with glass bottom having grids. These grids are clearly visible in imaging process through confocal microscopy. When the cofluency of cells in µ-dishes reaches to 80%, quantum dots can be introduced. Firstly quantum dot solution was filtered from 0.20 µm sterile filter and then the QD solution was mixed with the cells in the µ-dishes. Lastly, the cells were incubated 1-2 hours with CdS_xSe_{1-x} quantum dots in a dark cell incubator having 5% carbondioxide (CO_2) and 95% humidity at 37ºC. Concentration of quantum dots varied between 1 µg/ml and 10 µg/ml. When the concentration of quantum dots was higher than 10 µg/ml, cells were no longer adherent to surface of the flask, which was an indication of death of cells. Moreover, when the incubation time was longer than two hours, cells separated from the surface of the flask, loosing their health and growing state. When the incubation time was completed, the cells were washed with sterile phosphate buffer solution in order to remove the quantum dots which were freely suspended in the flask. Therefore, washing provided to get signals only from quantum

dots in the cellular environment. After washing process, the cells were ready to be imaged under confocal microscope.

3.2.2. Imaging of QDs in Live Cells Through Confocal Microscopy

A spinning disc confocal microscope shown in Figure 3.4 (Andor Revolution) equipped with a 100X oil-immersion objective was used to capture images of CdS_xSe_{1-x} quantum dots in live cells. Lateral resolution of microscope is 350 nm whereas axial resolution is 700 nm. Green laser was used to excite the green emitting quantum dots at 488 nm. An appropriate filter set was used to capture images.

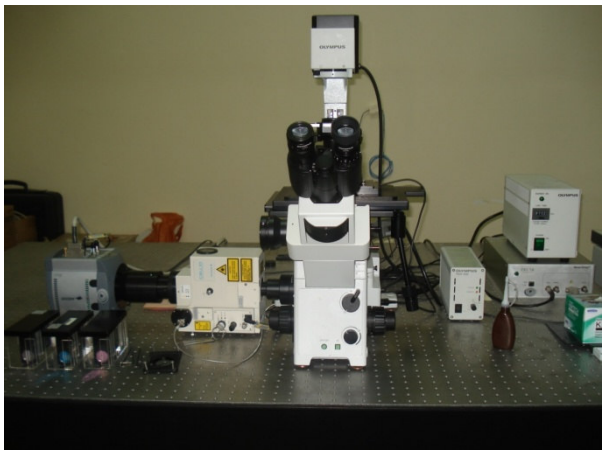

Figure 3.4. The confocal microscope used in this study (Andor Revolution).

3.2.3. Motion Analysis of Quantum Dots in Live Cells

In order to analyse motions of CdS_xSe_{1-x} quantum dots in A549 and BEAS-2B cells, an image processing program called ImageJ was used. ImageJ's functionality can be expanded through the use of plugins written in Java. In our experiments, Spot Tracker plugin was used.

3.3. Results

3.3.1. Localization and Intracellular Diffusion Pathways of QDs

Localization refers to the determination of position of quantum dots in cellular environment. Localization of quantum dots in live cells was quantified in order to determine the region where quantum dots were concentrated, gathering together. Diffusion is a principle way of movement of substances in cells, as well as the method for essential small molecules to cross through the cell membrane. It would be meaningful to study diffusion of quantum dots in cellular environment after verifying their positions in cells.

Figures 3.5, 3.6, 3.7 and 3.8 show the confocal microscope images of cells incubated with quantum dots. For each figure, the first image is the brigth field image, the second image is the confocal fluorescence image and the third image is the merged image of CdS_xSe_{1-x} quantum dots in live cells. Bright field image provides to determine the boundary of the cell. Flourescence image provides to determine position of the quantum dots through their fluorescence .

Figures 3.5 and 3.6 show representative confocal microscope images of MPA capped CdS_xSe_{1-x} quantum dots in A549 and BEAS-2B cells respectively. In the merged images, it can be clearly seen that the quantum dots entered to cell cytoplasm. They moved in the cytoplasm of the cell, not being stucked. In BEAS-2B cells fewer number of quantum dots were observed in the cell cytoplasm compared to A549 cells. Moreover, quantum dots are seemed to be present more homogeneous and brighter in A549 cells.

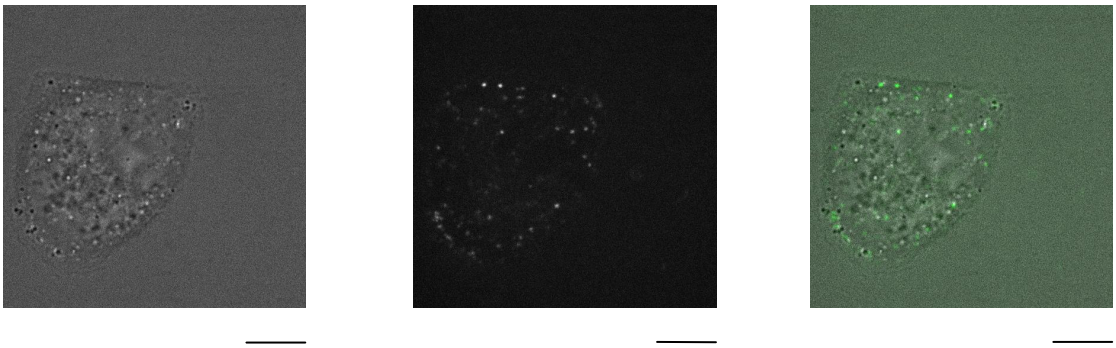

Figure 3.5. Bright field, confocal fuorescence and merged images of MPA capped gren emitting CdS_xSe_{1-x} quantum dots in live A549 cells, respectively. Bar is 10 μm.

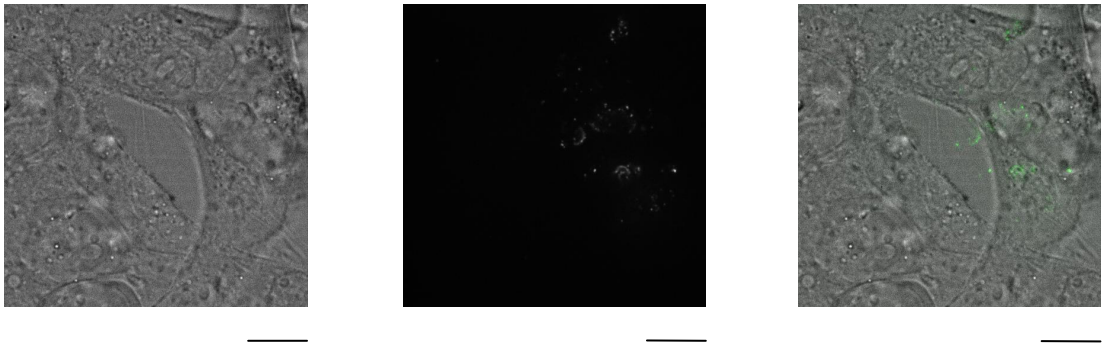

Figure 3.6. Bright field, confocal fuorescence and merged images of MPA capped green emitting CdS_xSe_{1-x} quantum dots in live BEAS-2B cells, respectively. Bar is 10 μm.

Figures 3.7 and 3.8 show confocal microscope images of NAC capped CdS_xSe_{1-x} quantum dots in A549 and BEAS-2B cells respectively. Merged confocal microscope images proved that the quantum dots were able to enter to the cell cytoplasm in two hours. They were observed to move in the cells. In the merged images, the quantum dots could be seen in the cellular environment. In A549 cells, we observed more quantum dots. It was understood that particles entered the cytoplasm of the A549 cells more easily than BEAS-2B cells. Moreover, NAC capped quantum dots were brighter in A549 cells than BEAS-2B cells which will be discussed a few parts later.

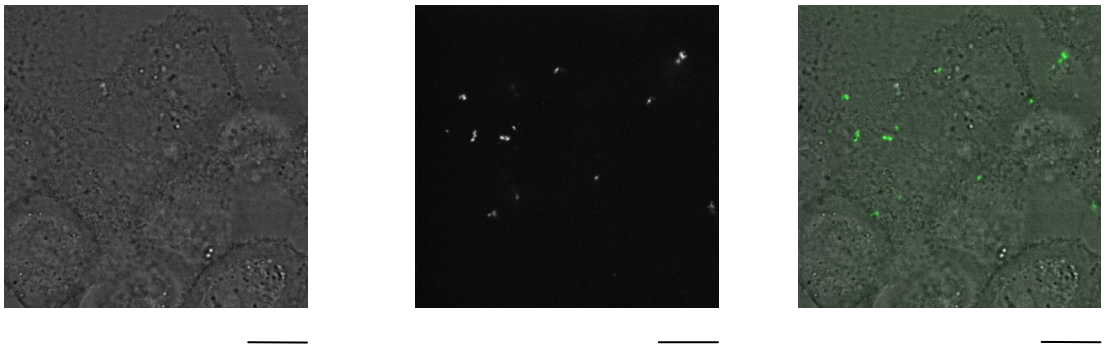

Figure 3.7. Bright field, confocal fuorescence and merged images of NAC capped green emitting CdS_xSe_{1-x} quantum dots in live A549 cells, respectively. Bar is 10 μm.

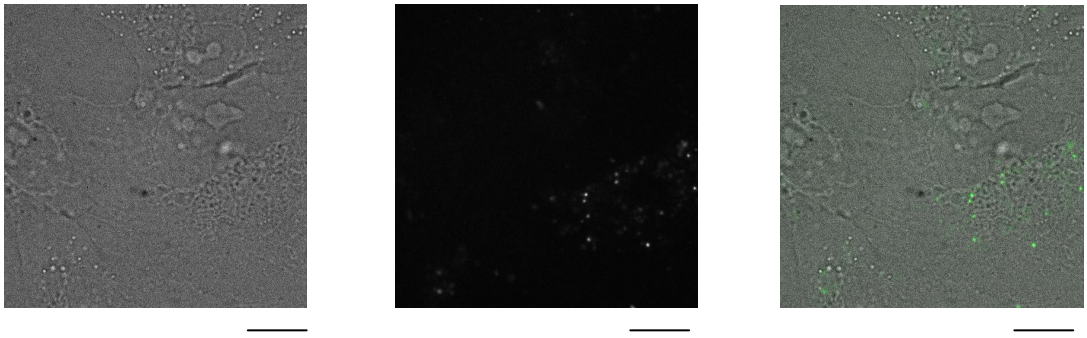

Figure 3.8. Bright field, confocal fuorescence and merged images of NAC capped green emitting CdS_xSe_{1-x} quantum dots in live BEAS-2B cells, respectively. Bar is 10 μm.

After determination of the location of MPA and NAC capped CdS_xSe_{1-x} quantum dots in A549 and BEAS-2B cells, it was aimed to figure out behaviour of quantum dots in a quantitative manner by tracking the motion of quantum dots in cells. For this purpose, ImageJ with Spot Tracker plug-in was used.

The positions of fluorescent spots were determined in each image and the two-dimensional trajectories of quantum dots were calculated using position of spots in x and y directions, as represented in Figure 1.4.

When spot position (x) vs spot position (y) is plotted, trajectories of quantum dots in live cells can be obtained. For MPA and NAC capped quantum dots, intracellular diffusion pathways were determined in A549 and BEAS-2B cells to understand what type of diffusion they undergo. From the Figures 3.9 and 3.10, we saw that MPA capped quantum dots performed various motions with different trajectories. We observed linear motion, constant motion, confined motion all together in a trajectory. As for the comparison of trajectories of MPA capped quantum dots in A549

and BEAS-2B cells, we observed that trajectories of quantum dots were more complex in A549 cells compared to BEAS-2B cell. This might be arised from the difference in diffusion constants of quantum dots in different cell lines which will be discussed in next part.

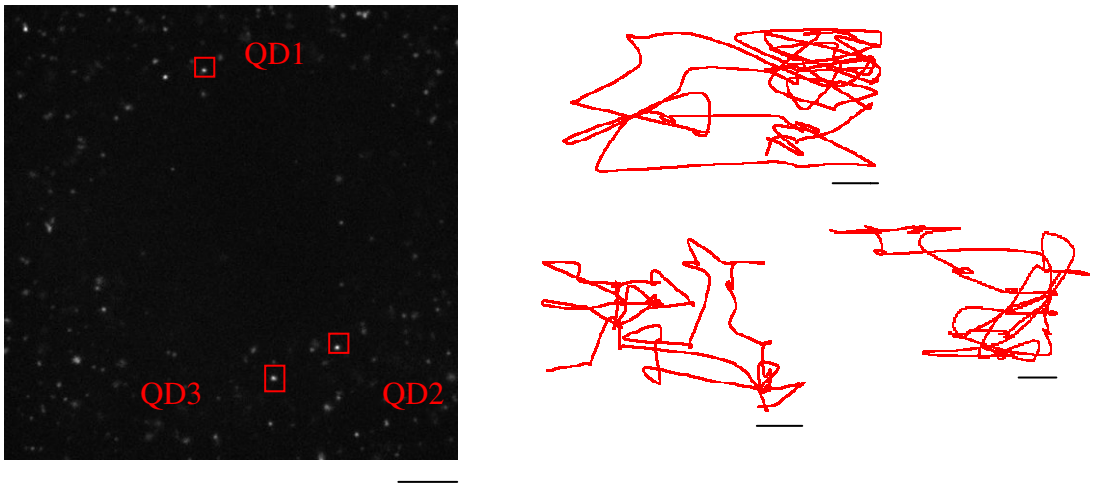

Figure 3.9. Confocal fluorescence image and trajectories of MPA capped green emitting CdS_xSe_{1-x} quantum dots in A549 cells. Bar under the figure is 10 µm. Bar under the trajectories is 100 nm.

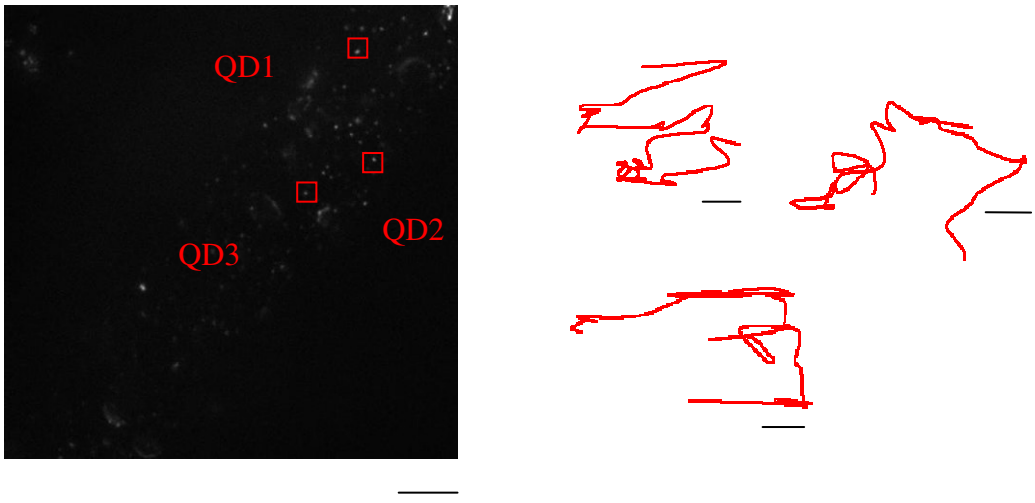

Figure 3.10. Confocal fluorescence image and trajectories of MPA capped green emitting CdS_xSe_{1-x} quantum dots in BEAS-2B cells. Bar under the figure is 10 µm. Bar under the trajectories is 100 nm.

Figures 3.11 and 3.12 show the trajectories of NAC capped CdS_xSe_{1-x} quantum dots in A549 and BEAS-2B cells respectively. All of the trajectories contained more

then one type of motions. Similar to MPA capped quantum dots, NAC capped quantum dots perform complicated motions in A549 cells compared to BEAS-2B cells.

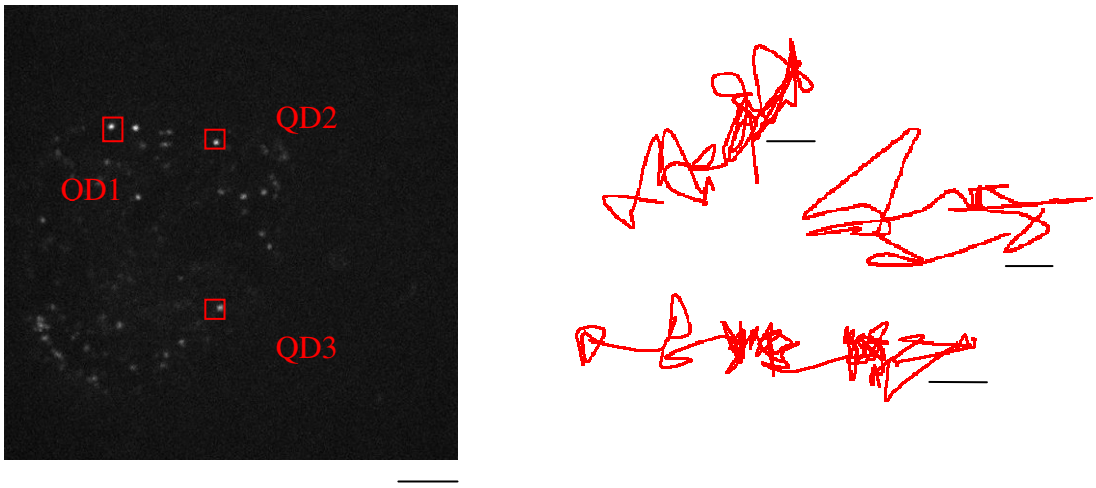

Figure 3.11. Confocal fluorescence image and trajectories of NAC capped green emitting CdS_xSe_{1-x} quantum dots in A549 cells. Bar under the figureis 10 µm. Bar under the trajectories is 100 nm.

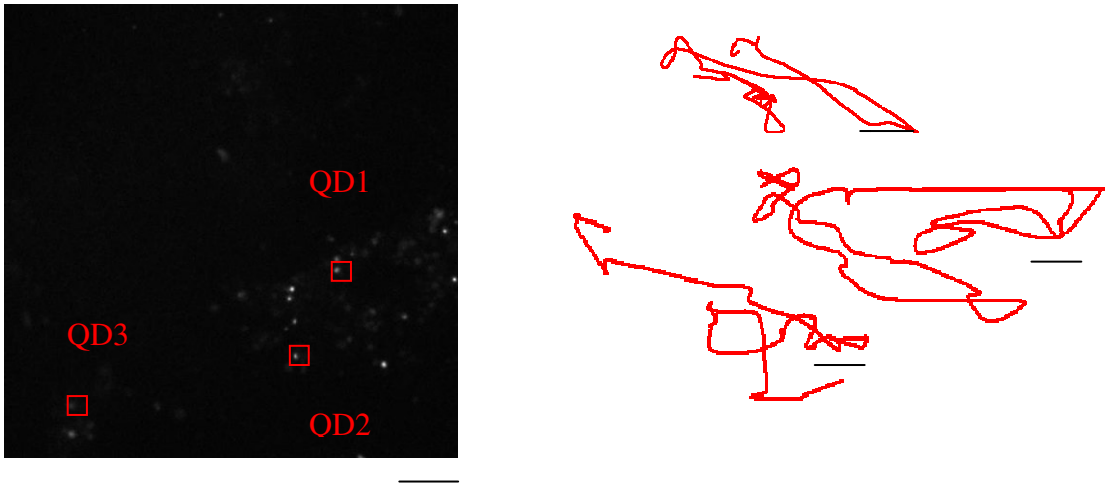

Figure 3.12. Confocal fluorescence image and trajectories of NAC capped green emitting CdS_xSe_{1-x} quantum dots in BEAS-2B cells. Bar under the figure is 10 µm. Bar under the trajectories is 100 nm.

3.3.2. Mean Square Displacement of Quantum Dots

Mean square displacement (MSD) is a measure of the average distance a molecule travels. One of the main purposes of MSD analysis is the evaluation of the

diffusion coefficient value (D) and to estimate the type of diffusion undergone by the particle.

For each trajectory of a quantum dot, the two dimensional mean square displacement (MSD) was calculated according to the Equation 3.1 (Bannai et al. 2006).

$$MSD(n\tau) = \frac{1}{N-n}\sum_{i=1}^{N-n}[(x((i+n)\tau - x(i\tau))^2 - (y((i+n)\tau - y(i\tau))^2] \quad (3.1)$$

where τ is the acquisition time, n is the square where particle exists and N is the total number of frames.

It is important to realize that if the molecule is undergoing multiple types of diffusion during the observed trajectory, the extracted value will be an average one because a single diffusion constant is extracted from such an analysis. For example, if the molecule undergoes slow diffusion during the first half of the trajectory, followed by faster diffusion during the second half, the measured average diffusion constant will tell nothing about the underlying two very different diffusion coefficients and will be biased toward the larger value (Saxton et al. 1997). Several methods have been proposed to detect or analyze trajectories that may comprise different diffusion regimes. Different types of motion can be distinguished from the time dependence of the MSD graph. For simple two-dimensional Brownian motion, the MSD versus time plot is linear with a slope of 4D, where D is the diffusion constant. If the MSD versus time plot tends toward a constant value L, the diffusion is confined in a domain of size $\sim$ L.

In Figure 3.13, MSD plot was drawn for MPA capped CdS_xSe_{1-x} quantum dots in A549 cells. In the plot, we did not observe a linear trend. It was observed that slope of the line increased and than decreased which meant that quantum dots speeded up, reached a maximum mean square displacement and then slowed down and stopped.

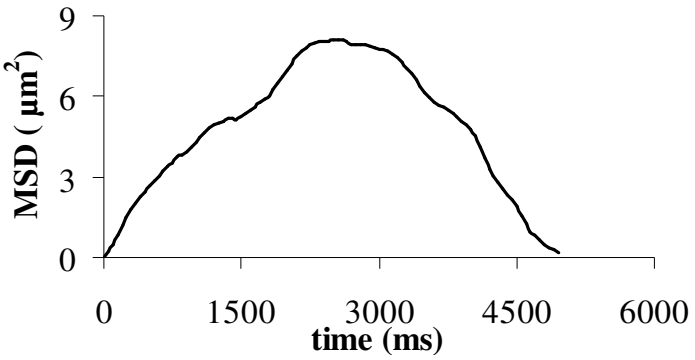

Figure 3.13. MSD plot of MPA capped green emitting CdS_xSe_{1-x} quantum dots in A549 cells.

In Figure 3.14 MSD plot was drawn for MPA capped CdS_xSe_{1-x} quantum dots in BEAS-2B cells. The same trend was observed for quantum dots in BEAS-2B cells: quantum dots were accelerating and than decelerating. Diffusion area of MPA capped quantum dots in A549 cells was larger than that of BEAS-2B cells. This difference might arise from the biomolecule to which quantum dots binds.

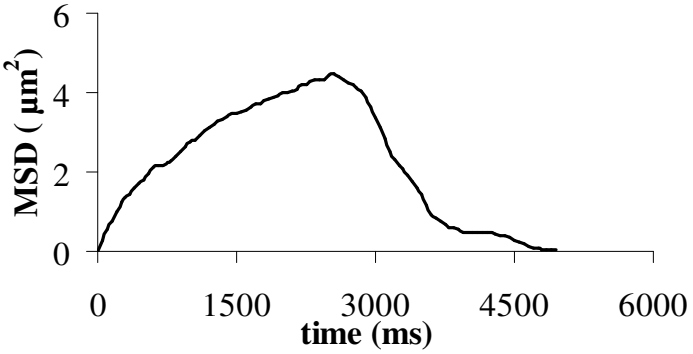

Figure 3.14. MSD plot of MPA capped green emitting CdS_xSe_{1-x} quantum dots in BEAS-2B cells.

In Figures 3.15 and 3.16 MSD plots were drawn for NAC capped CdS_xSe_{1-x} quantum dots in A549 and BEAS-2B cells respectively.

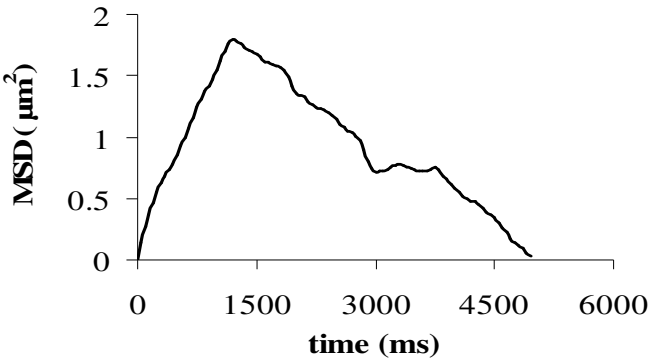

Figure 3.15. MSD plot of NAC capped green emitting CdS_xSe_{1-x} quantum dots in A549 cells.

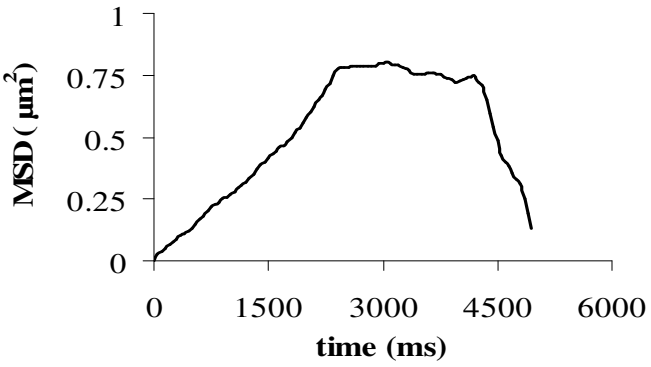

Figure 3.16. MSD plot of NAC capped green emitting CdS_xSe_{1-x} quantum dots in BEAS-2B cells.

As for the comparison of diffusion of quantum dots in cells, we can say that both MPA and NAC capped quantum dots diffused in a highly restricted domain in BEAS-2B cells. Moreover, diffusion area of MPA capped quantum dots was larger than that of NAC capped quantum dots in both A549 and BEAS-2B cells. The maximum diffusion area was observed for MPA capped quantum dots in A549 cells while the minimum diffusion area was observed for NAC capped quantum dots in BEAS-2B cells.

3.3.3. Diffusion Coefficients of Quantum Dots

The diffusion coefficient (D) is determined by fitting the initial few points of the MSD versus time curve with the equation of MSD(t) = 4Dt + b. It is generally preferred to use this fit because of the fact that it provides to determine D independently of the type of motion. In our calculations, we used initial four points of MSD vs time graph.

Slope of this line was divided by four and diffusion coefficients were calculated. If particles undergo more than one type of motion, there would be observed more than one linear region in the MSD versus time graph.

In Figures 3.17 and 3.18 histogram of diffusion coefficients of MPA capped CdS_xSe_{1-x} quantum dots in A549 and BEAS-2B cells are seen respectively. For A549 cells, we observed a trimodal distribution showing different type of motions. 60% of MPA capped CdS_xSe_{1-x} quantum dots moved with a diffusion coefficient of 50 $\mu m^2/s$. Quantum dots diffused with two other velocity distribution averaging 175 $\mu m^2/s$ and 425 $\mu m^2/s$.

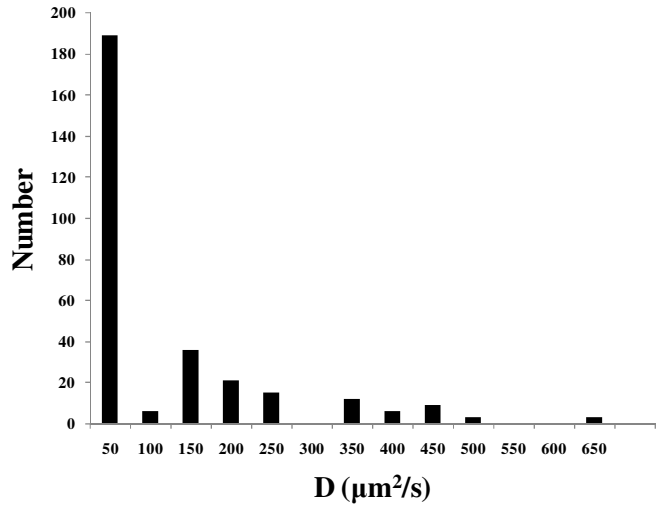

Figure 3.17. Histogram of diffusion coefficients of MPA capped green emitting CdS_xSe_{1-x} quantum dots in A549 cells (N=300).

In BEAS-2B cells, we observed multimodal distribution. It means that, there was various type of diffusion. 37% of the MPA capped quantum dots diffused with a diffusion constant of 50 $\mu m^2/s$. Only 3% of the quantum dots had the highest diffusion coefficient, 650 $\mu m^2/s$.

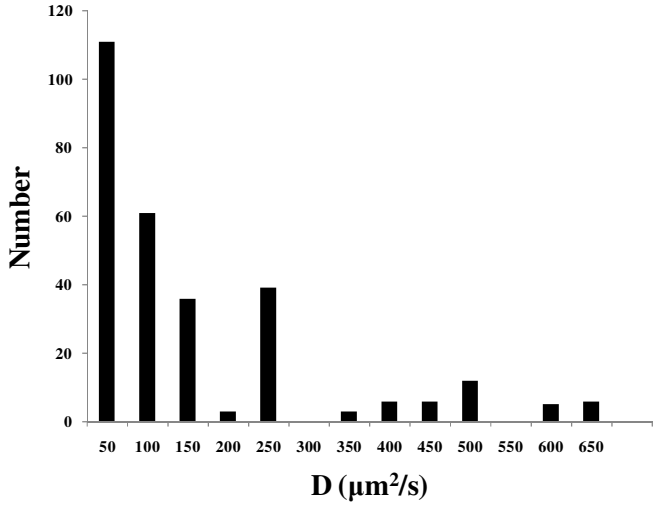

Figure 3.18. Histogram of diffusion coefficients of MPA capped green emitting CdS_xSe_{1-x} quantum dots in BEAS-2B cells (N=282).

In Figures 3.19 and 3.20 histogram of diffusion coefficients of NAC capped CdS_xSe_{1-x} quantum dots in A549 and BEAS-2B cells are seen respectively. In A549 cells, we observed a unimodal distribution showing that nanocrystals were almost immobile due to amine and acetyl groups of NAC. When the diffusion coefficients were calculated for NAC capped quantum dots, it was observed that the 96% of the NAC capped quantum dots had diffusion coefficient of 50 $\mu m^2/s$. They diffused very slowly in A549 cells. In BEAS-2B cells, NAC capped quantum dots exhibited multimodal distribution. 60% of NAC capped quantum dots had a diffusion coefficient of 50 $\mu m^2/s$.

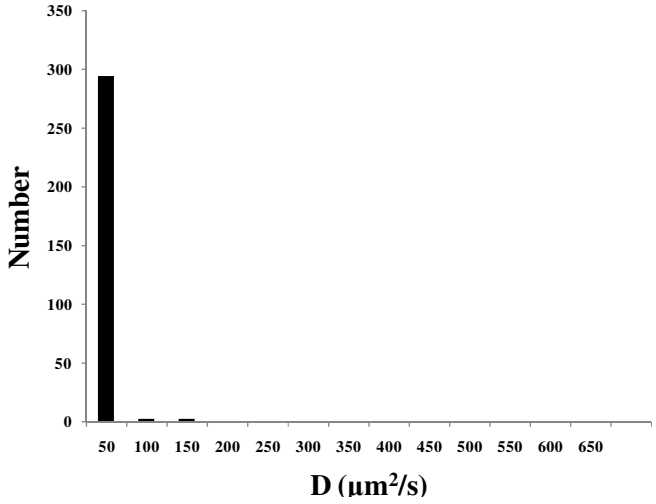

Figure 3.19. Histogram of diffusion coefficients of NAC capped green emitting CdS_xSe_{1-x} quantum dots in A549 cells (N=300).

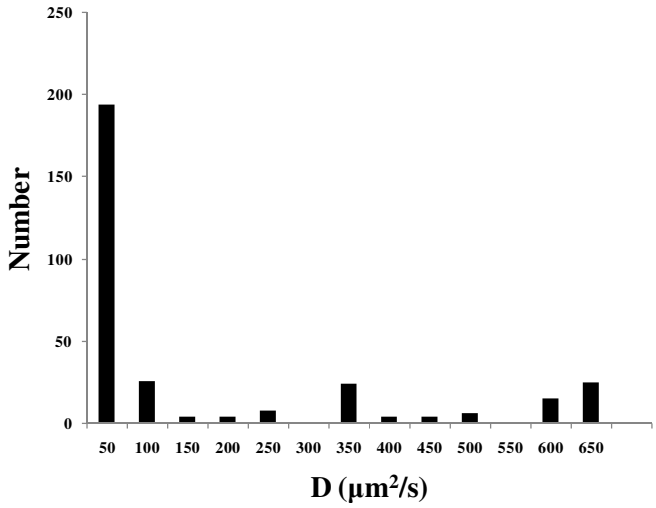

Figure 3.20. Histogram of diffusion coefficients of NAC capped green emitting CdS_xSe_{1-x} quantum dots in BEAS-2B cells (N=314).

3.3.4. Intensity Analysis

Another point to be considered is photobleaching, commonly referred as fading. Fluorescence emitted by almost all fluorophores fades during observation. This is called photobleaching or dye photolysis and it involves a photochemical modification of dye causing the irreversible lost of its ability to fluoresce. Indeed, fluorophores in the excited state may undergo chemical or biochemical reaction that lead to their rapid

degradation and destruction and consequent loss of image quality during measurement. In a certain sense fluorophores are consumed by being observed.

We plotted intensity versus time graphs for MPA and NAC capped CdS_xSe_{1-x} quantum dots in live A549 and BEAS-2B cells.

Figures 3.21 and 3.22 show fluorescence intensity of MPA capped CdS_xSe_{1-x} quantum dots in A549 and BEAS-2B cells respectively. As it is seen fluorescence intensity of MPA capped CdS_xSe_{1-x} quantum dot is around 200 counts per 100 ms. Background intensity was around 90, so we surely concluded that this intensity signal came from the fluorescence quantum dot. It is quite clear that intensity of the quantum dot did not decrease over time which means that we did not observe any photobleaching during experimental measurements.

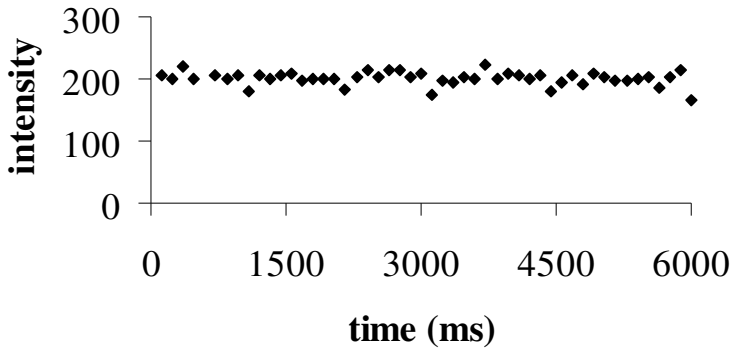

Figure3.21. Fluorescence intensities of MPA capped green emitting CdS_xSe_{1-x} quantum dots in A549 cells. Intensity is equal to count/100 ms.pixel.

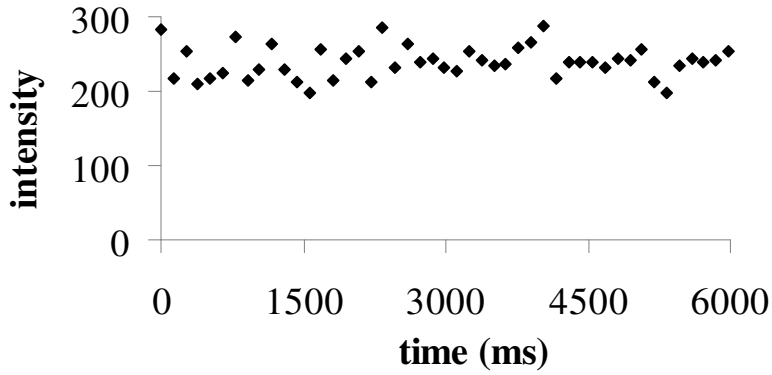

Figure3.22. Fluorescence intensities of MPA capped green emitting CdS_xSe_{1-x} quantum dots in BEAS-2B cells. Intensity is equal to count/100 ms.pixel.

Figures 3.23 and 3.24 show intensity of NAC capped CdS_xSe_{1-x} quantum dots in A549 and BEAS-2B cells respectively. For NAC capped quantum dots, no photobleaching behaviour was observed. Intensity was constant over time which is a great advantage of quantum dots that allowed us to perform long term observations.

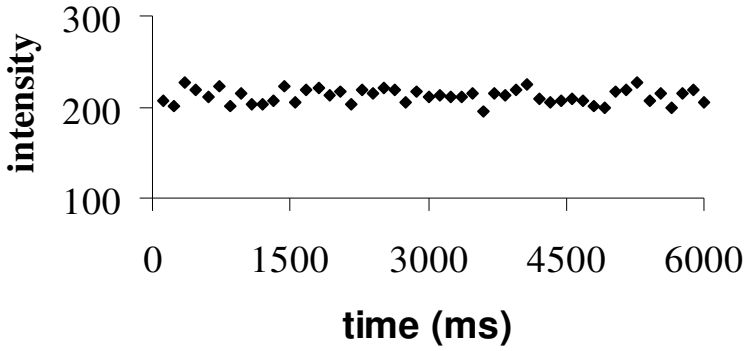

Figure 3.23. Fluorescence intensities of NAC capped green emitting CdS_xSe_{1-x} quantum dots in A549 cells. Intensity is equal to count/100 ms.pixel.

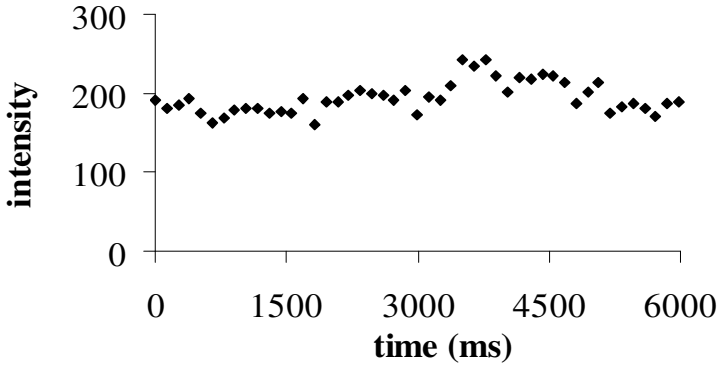

Figure 3.24. Fluorescence intensities of NAC capped green emitting CdS_xSe_{1-x} quantum dots in BEAS-2B cells. Intensity is equal to count/100 ms.pixel.

Moreover it is necessary to prove that analyzed CdS_xSe_{1-x} quantum dots were single. For that purpose we created intensity versus number histograms for CdS_xSe_{1-x} quantum dots. Figures 3.25 and 3.26 shows fluorescence intensity histograms for MPA capped CdS_xSe_{1-x} quantum dots in A549 and BEAS-2B cells respectively. We observed monodisperse distribution and it is also Gaussian shaped indicating the presence of

single quantum dots. Most of the MPA capped CdS_xSe_{1-x} quantum dots have intensity value of 200 count.

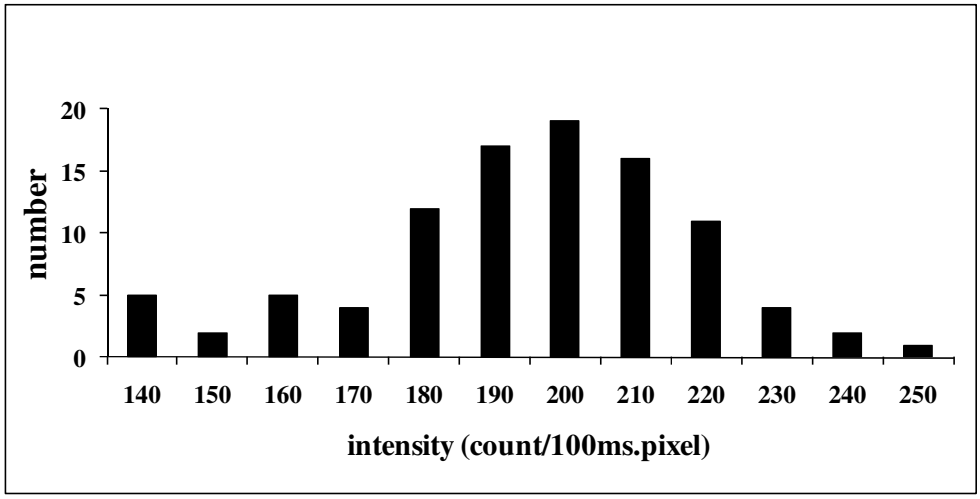

Figure 3.25. Fluorescence intensity histogram of MPA capped green emitting CdS_xSe_{1-x} quantum dots in A549 cells (N=98).

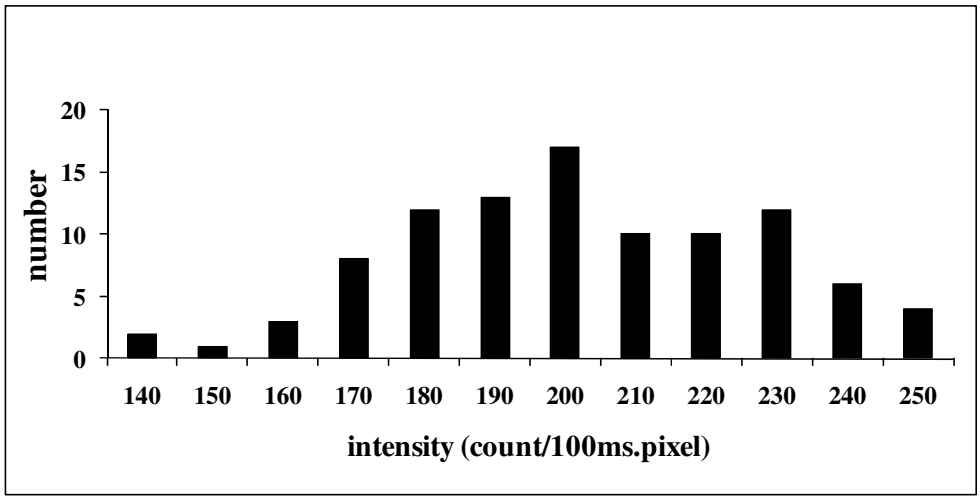

Figure 3.26. Fluorescence intensity histogram of MPA capped green emitting CdS_xSe_{1-x} quantum dots in BEAS-2B cells (N=98).

Figures 3.27 and 3.28 show fluorescence intensity histograms for NAC capped CdS_xSe_{1-x} quantum dots in A549 and BEAS-2B cells respectively. Most of the quantum dots appear with a intensity value of 190 count. Similar to MPA capped CdS_xSe_{1-x} quantum dots, monodisperse Gaussian distribution was observed as an indication of single quantum dots.

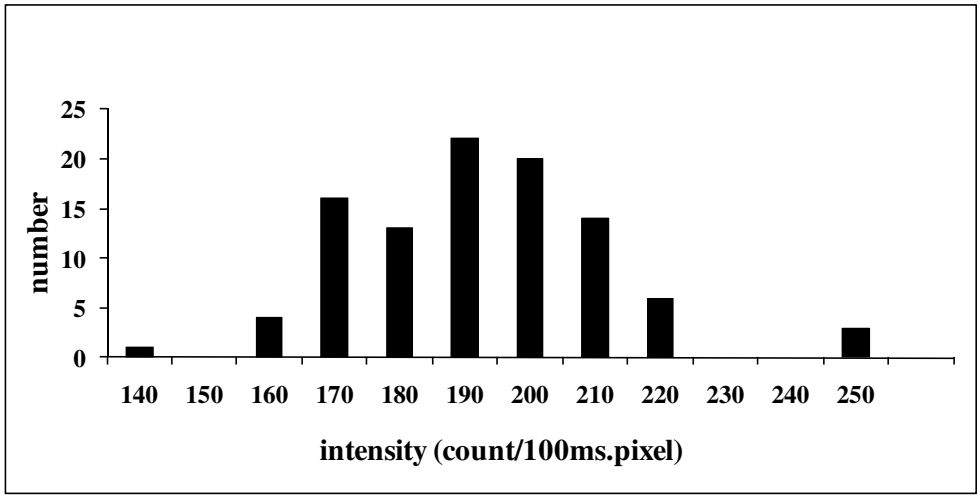

Figure 3.27. Fluorescence intensity histogram of NAC capped green emitting CdS_xSe_{1-x} quantum dots in A549 cells (N=100).

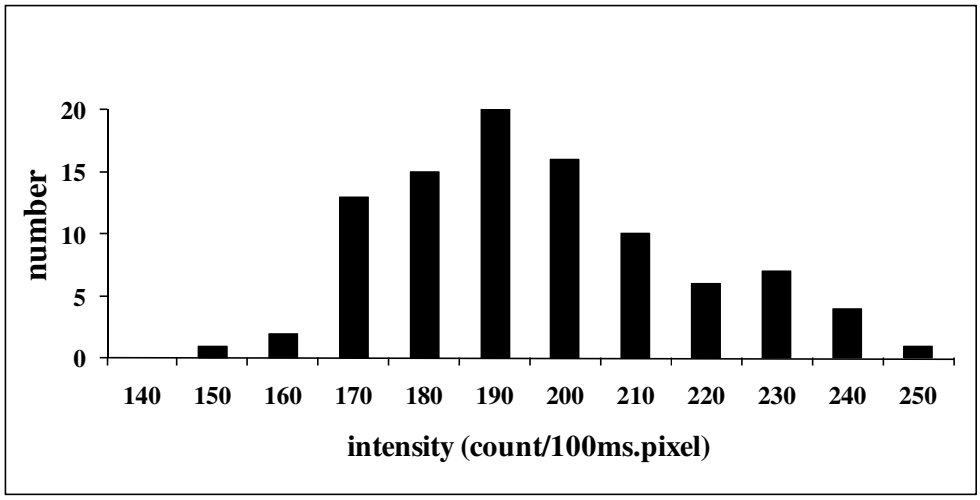

Figure 3.28. Fluorescence intensity histogram of NAC capped green emitting CdS_xSe_{1-x} quantum dots in BEAS-2B cells (N=99).

3.4. Discussion

It is crucial to focus on numerous factors influence behaviour of quantum dots in cellular environment. Depending on surface chemistry and cell type; localization, diffusion and intracellular trajectories of quantum dots in live cells differ.

Firstly, it must be proven that quantum dots are able to enter the cells. Many nanomaterials were observed to be localized in cells. CdSe/ZnS core shell quantum dots

were successfully incorporated to cells and they were internalized into the cytoplasm of the cells (Zhang et al. 2009). In another study CdSe/ZnS-PEG-COOH quantum dots were observed to be in a perinuclear region compatible with endosomal/lysosomal localization but none of the quantum dots were observed in the cell nucleus (Damalakiene et al. 2009). According to our confocal microscopy images, MPA and NAC capped CdS_xSe_{1-x} quantum dots were observed to enter the cell cytoplasm but they were not able to enter the nucleus of the whether A549 or BEAS-2B cells. It is needed to stain cytoplasm and cell membrane to ensure the presence of quantum dots in the cytoplasm of the cells.

Moreover, it is very important to determine optimum quantum dot concentration and incubation time for cellular environment in order to keep cells healthy and growing without damaging. Damalakiene and coworkers stated that time for internalization of quantum dots into cells varied from five minutes to eighteen hours (Damalakiene et al. 2009). According to our studies, CdS_xSe_{1-x} quantum dots could enter the cellular environment only one hour after incubation with quantum dots. However we observed that, when the incubation period was longer than two hours, cells started to be removed from the flask showing that quantum dots induce toxicity.

After determination of positions of quantum dots in live A549 and BEAS-2B cells, it was aimed to determine intracellular trajectories of quantum dots. Trejectories give idea about the type of diffusion a molecule undergoes. Mainly there are four types of diffusions: simple, directed, restricted and stationary diffusion (Kusumi et al. 1993). In our experiment, we observed that MPA and NAC capped CdS_xSe_{1-x} quantum dots performed various types of motions: in a trajectory, we observed confined motion, linear motion and directed motion. However, NAC capped quantum dots performed notable directed motion compared to MPA capped quantum dots.

Mean square displacement (MSD)-Δtime (t) plots are important to determine diffusion constants and diffusion types of molecules. If the slope of MSD-Δt plot is linear, molecules undergo simple diffusion. If the plot is parabolic then diffusion is directed (Kusumi et al. 1993). MSD-Δt plots of MPA and NAC capped CdS_xSe_{1-x} quantum dots were neither linear nor parabolic. For each cell type, it was observed that quantum dots speeded up and then slowed down reaching to their initial position in the cells. This behaviour may be speculated that quntum dots may bind to a biomolecule which made the diffusion limited.

Using slope MSD-Δt plot, the diffusion coefficient were calculated for the CdS_xSe_{1-x} quantum dots in the cellular environment. For the MPA capped CdS_xSe_{1-x} quantum dots trimodal distribution was observed in A549 cells. It was meant that the MPA capped quantum dots performed different types of motions in A549 cells. However, NAC capped quantum dots were exhibited unimodal distribution. It meant that NAC capped quantum dots were almost immobile in A549 cells due to amine and acetyl groups of NAC. In BEAS-2B cells, both MPA and NAC capped quantum dots performed multimodal distributions. In all experiments, diffusion coefficient were in the range of $5x10^{-7}$ cm^2/s to $65x10^{-7}$ cm^2/s. Kusumi and coworkers stated that, molecules having a diffusion coefficient smaller than $4.6x10^{-12}$ cm^2/s undergo stationary diffusion.

Another point is the intensity of quantum dots. Impressive photostability and high resistance against photobleaching make quantum dots superior to current fluorophores and allow long term observation (Drbohlavova et al. 2009). Synthesized CdS_xSe_{1-x} quantum dots meeted these criteria: quntum dots having 20% quantum yield were seen very fluorescent spots under confocal microscope and we observed no photobleaching during imaging studies. Moreover, intensity of the quantum dots was two times of background intensity.

Intensity versus number histograms give information about the presence of single quantum dots. In intensity versus number histograms, monodisperse Gaussian distribution was observed. It meant that we observed single CdS_xSe_{1-x} quantum dots in both A549 and BEAS-2B cells.

3.5. Conclusion

In this study, 3-mercaptopropionic acid (MPA) and N-acetyl-L-cysteine (NAC) capped CdS_xSe_{1-x} alloy quantum dots were used. Human lung adenocarcinoma epithelial (A549) cells and human bronchial epithelial (BEAS-2B) cells were incubated with CdS_xSe_{1-x} quantum dots. Incubation period was one-two hours and concentration of CdS_xSe_{1-x} was between 1 μg/mL and 10 μg/mL. Positions and real time motions of quantum dots were tracked using a spinning disc confocal microscope under 488 nm illumination. The center of fluorescent spots of quantum dots was determined by two dimensional Gaussian fitting by sub-pixel resolution. The intracellular diffusion

pathways, mean square displacement, diffusion coefficients and size of domains in which quantum dots made motions were analyzed by ImageJ plugin Spot Tracker. Confocal microscope images proved that quantum dots were able to enter the cell cytoplasm. MPA capped CdS_xSe_{1-x} quantum dots performed trimodal diffusion in A549 cells showing different type of motions whereas NAC capped quantum dots exhibited unimodal diffusion showing that quantum dots were almost immobile due to the amine and acetyl groups of NAC. In BEAS-2B cells, quantum dots made various types of motions. As a result, quantum dots performed different types of motion in cellular environment depending on both surface chemistry and cell type. What is common for all experiments was that there was no decrease in the intensity of quantum dots in cells. Moreover we were able to observe single CdS_xSe_{1-x} quantum dots. Presence of single quantum dots was proved using the intensity versus number histograms which had monodisperse Gaussian distribution.

REFERENCES

Abramowitz, Mortimer. 2006. Microscope : Basics and Beyond. In *Scanning*. New York.

Adams, M. C., W. C. Salmon, S. L. Gupton, C. S. Cohan, T. Wittmann, N. Prigozhina, and C. M. Waterman-Storer. 2003. A high-speed multispectral spinning-disk confocal microscope system for fluorescent speckle microscopy of living cells. *Methods* 29 (1):29-41.

Amin, R., S. Hwang, and S. H. Park. 2011. Nanobiotechnology: An interface between nanotechnology and biotechnology. *Nano* 6 (2):101-111.

Bannai, H., S. Levi, C. Schweizer, M. Dahan, and A. Triller. 2006. Imaging the lateral diffusion of membrane molecules with quantum dots. *Nature Protocols* 1 (6):2628-2634.

Biju, V., T. Itoh, and M. Ishikawa. 2010. Delivering quantum dots to cells: bioconjugated quantum dots for targeted and nonspecific extracellular and intracellular imaging. *Chemical Society Reviews* 39 (8):3031-3056.

Borrelli, N. F. 2003. Semiconductor Nanocrystals From Basic Principles to Applications.

Buhro, W. E., and V. L. Colvin. 2003. Semiconductor nanocrystals - Shape matters. *Nature Materials* 2 (3):138-139.

Bruchez, M., M. Moronne, P. Gin, S. Weiss, and A. P. Alivisatos. 1998. Semiconductor nanocrystals as fluorescent biological labels. *Science* 281 (5385):2013-2016.

Chong, F. K., C. G. Coates, D. J. Denvir, N. McHale, K. Thornbury, and M. Hollywood. 2004. Optimization of spinning disk confocal microscopy: Synchronization with the ultra-sensitive EMCCD. In *Three-Dimensional and Multidimensional Microscopy: Image Acquisition and Processing Xi*, edited by J. A. Conchello, C. H. Cogswell and T. Wilson.

Damalakiene, Leona, Saulius Bagdonas, and Ricardas Rotomskis. 2009. Influence of Growth Factor on Internalization Pathway of Quantum Dots into Cells. *IEEE NANO Organizers*:978-981.

Drbohlavova, J., V. Adam, R. Kizek, and J. Hubalek. 2009. Quantum Dots - Characterization, Preparation and Usage in Biological Systems. *International Journal of Molecular Sciences* 10 (2):656-673.

Ethayaraja, M., C. Ravikumar, D. Muthukumaran, K. Dutta, and R. Bandyopadhyaya. 2007. CdS-ZnS core-shell nanoparticle formation: Experiment, mechanism, and simulation. *Journal of Physical Chemistry C* 111 (8):3246-3252.

Evident Home Page. www.evidenttech.com (accessed June 2011).

Gu, Z. Y., L. Zou, Z. Fang, W. H. Zhu, and X. H. Zhong. 2008. One-pot synthesis of highly luminescent CdTe/CdS core/shell nanocrystals in aqueous phase. *Nanotechnology* 19 (13).

Jamieson, T., R. Bakhshi, D. Petrova, R. Pocock, M. Imani, and A. M. Seifalian. 2007. Biological applications of quantum dots. *Biomaterials* 28 (31):4717-4732.

Joshi, A., K. Y. Narsingi, M. O. Manasreh, E. A. Davis, and B. D. Weaver. 2006. Temperature dependence of the band gap of colloidal CdSe/ZnS core/shell nanocrystals embedded into an ultraviolet curable resin. *Applied Physics Letters* 89 (13):-.

Kluson, P., M. Drobek, H. Bartkove, and I. Budil. 2007. Welcome to the nanoworld (vol 101, pg 262, 2007). *Chemicke Listy* 101 (7):591-591.

Kral, V., J. Sotola, P. Neuwirth, Z. Kejik, K. Zaruba, and P. Martasek. 2006. Nanomedicine - Current status and perspectives: A big potential or just a catchword? *Chemicke Listy* 100 (1):4-9.

Kusumi, A., Y. Sako, and M. Yamamoto. 1993. Confined lateral diffusion of membrane receptors as studied by single particle tracking (nanovid microscopy) effects of calcium induced differentiation in cultured epithelial cells. *Biophysical Journal* 65 (5):2021-2040.

Liang, G. X., L. L. Li, H. Y. Liu, J. R. Zhang, C. Burda, and J. J. Zhu. 2010. Fabrication of near-infrared-emitting CdSeTe/ZnS core/shell quantum dots and their electrogenerated chemiluminescence. *Chemical Communications* 46 (17):2974-2976.

Lichtman, J. W., and J. A. Conchello. 2005. Fluorescence microscopy. *Nature Methods* 2 (12):910-919.

Masters, John R. W. 2000. Animal Cell Culture

Minsky, M. 1988. Memoir on inventing the confocal scanning microscope. *Scanning* 10 (4):128-138.

Pan, D. C., Q. Wang, S. C. Jiang, X. L. Ji, and L. J. An. 2005. Synthesis of extremely small CdSe and highly luminescent CdSe/CdS core-shell nanocrystals via a novel two-phase thermal approach. *Advanced Materials* 17 (2):176-+.

Pan, D. C., Q. Wang, S. C. Jiang, X. L. Ji, and L. J. An. 2007. Low-temperature synthesis of oil-soluble CdSe, CdS, and CdSe/CdS core - Shell nanocrystals by using various water-soluble anion precursors. *Journal of Physical Chemistry C* 111 (15):5661-5666.

Pecharsky, Vitalij; Zavalij, Peter 2008. *Fundamentals of Powder Diffraction and Structural Characterization of Materials* 2ed: Springer.

Petros, R. A., DeSimone, J. M. 2010. Strategies in the design of nanoparticles for therapeutic applications. *Nat Rev Drug Discov*. 9 (8):615-27.

Prasad, V., D. Semwogerere, and E. R. Weeks. 2007. Confocal microscopy of colloids. *Journal of Physics-Condensed Matter* 19 (11).

Regulacio, M. D., and M. Y. Han. 2010. Composition-Tunable Alloyed Semiconductor Nanocrystals. *Accounts of Chemical Research* 43 (5):621-630.

Sayes, C. M., J. D. Fortner, W. Guo, D. Lyon, A. M. Boyd, K. D. Ausman, Y. J. Tao, B. Sitharaman, L. J. Wilson, J. B. Hughes, J. L. West, and V. L. Colvin. 2004. The differential cytotoxicity of water-soluble fullerenes. *Nano Letters* 4 (10):1881-1887.

Semwogerere, Denis, and Eric R. Weeks. 2005. Confocal Microscopy. *Encyclopedia of Biomaterials and Biomedical Engineering*.

Swafford, L. A., L. A. Weigand, M. J. Bowers, J. R. McBride, J. L. Rapaport, T. L. Watt, S. K. Dixit, L. C. Feldman, and S. J. Rosenthal. 2006. Homogeneously alloyed CdSxSe1-(x) nanocrystals: Synthesis, characterization, and composition/size-dependent band gap. *Journal of the American Chemical Society* 128 (37):12299-12306.

Vibin, M., R. Vinayakan, A. John, C. S. Rejiya, V. Raji, and A. Abraham. 2011. Cellular uptake and subcellular localization of highly luminescent silica-coated CdSe quantum dots - In vitro and in vivo. *Journal of Colloid and Interface Science* 357 (2):366-371.

Wang, Ying, Zhiyong Tang, and Nicholas A. Kotov. 2005. Bioapplication of Nanosemiconductors. *nanotoday*.

Zhang, J. G., N. Coombs, E. Kumacheva, Y. K. Lin, and E. H. Sargent. 2002. A new approach to hybrid polymer-metal and polymer-semiconductor particles. *Advanced Materials* 14 (23):1756-+.

Zhang, T. L., Y. S. Xia, X. L. Diao, and C. Q. Zhu. 2008. Preparation and formation mechanism of strong violet luminescent CdS quantum dots by using a ligand exchange strategy. *Journal of Nanoparticle Research* 10 (1):59-67.

Zhang, L. W., and N. A. Monteiro-Riviere. 2009. Mechanisms of Quantum Dot Nanoparticle Cellular Uptake. *Toxicological Sciences* 110 (1):138-155.